Supporting information for: Modified Entropy Scaling of the Transport Properties of the Lennard-Jones Fluid

Ian H. Bell,[*,†] Richard Messerly,[†] Monika Thol,[‡] Lorenzo Costigliola,[¶] and Jeppe C. Dyre[¶]

†*Applied Chemicals and Materials Division, National Institute of Standards and Technology, Boulder, CO 80305*

‡*Thermodynamics, Ruhr-Universität Bochum, Universitätsstraße 150, 44801 Bochum, Germany*

¶*DNRF Centre "Glass and Time," IMFUFA, Department of Science and Environment, Roskilde University, Postbox 260, DK-4000 Roskilde, Denmark*

E-mail: ian.bell@nist.gov

Contents

1 Potential Agnostic Derivations **S3**

1.1 Derivation of s_{ex} and its derivatives . . . S3

1.2 Dilute gas limit . . . S5

1.3 2/3 is Special . . . S6

1.4 Dilute Gas Correction Terms . . . S7

1.5 Critical Enhancement to Conductivity . . . S7

2 Data Analysis **S8**

2.1 Data Tables . . . S8

3 Larger figures **S13**

3.1 Rosenfeld scaling . . . S13

3.2 Novel scaling . . . S15

3.3 Uncertainty in D . . . S17

3.4 Data plots . . . S18

3.4.1 Thermal Conductivity . . . S18

3.4.2 Self-Diffusion . . . S19

3.4.3 Viscosity . . . S21

3.5 Correction term of Yeh and Hummer . . . S23

4 Inverse Power Law Potential **S24**

4.1 Thermodynamics . . . S24

4.2 Derivations of IPL hardness terms . . . S24

4.3 Collision Integral . . . S25

4.4 Scaled zero-density transport properties . . . S26

4.4.1 Python/sympy code for calculating A_l . . . S29

5 The High-Temperature Limit **S30**

5.1 Rosenfeld re-derivation S32

6 EoS from Thol et al. **S33**

6.1 Virial coefficients S33

7 Comparisons with existing correlations from the literature **S36**

7.1 Viscosity S37

7.2 Conductivity S40

7.3 Self-Diffusion S43

8 Verification Data **S45**

References **S47**

1 Potential Agnostic Derivations

1.1 Derivation of s_{ex} and its derivatives

The equation of state for any fluid at low and moderate densities can be written in virial expansion form as

$$Z \equiv \frac{p}{\rho_{\mathrm{N}} k_{\mathrm{B}} T} = 1 + \sum_{m=2}^{\infty} B_m(T) \rho_{\mathrm{N}}^{m-1}, \tag{1}$$

The reduced residual Helmholtz energy is given by

$$\begin{aligned}
\alpha^{\mathrm{r}} &= \frac{a^{\mathrm{r}}}{k_{\mathrm{B}} T} && (2)\\
&= \int_0^{\rho_{\mathrm{N}}} \frac{Z-1}{\rho_{\mathrm{N}}} d\rho_{\mathrm{N}} && (3)\\
&= \int_0^{\rho_{\mathrm{N}}} \left[\sum_{m=2}^{\infty} B_m(T) \rho_{\mathrm{N}}^{m-2} \right] d\rho_{\mathrm{N}} && (4)\\
&= \sum_{m=2}^{\infty} \frac{1}{m-1} B_m(T) \rho_{\mathrm{N}}^{m-1} && (5)\\
&= B_2 \rho_{\mathrm{N}} + \frac{1}{2} B_3 \rho_{\mathrm{N}}^2 + \ldots && (6)
\end{aligned}$$

and the excess entropy is then obtained from

$$\frac{1}{k_\mathrm{B}}\left(\frac{\partial a^\mathrm{r}}{\partial T}\right)_{\rho_\mathrm{N}} = -\frac{s_\mathrm{ex}}{k_\mathrm{B}} = T\left(\frac{\partial \alpha^\mathrm{r}}{\partial T}\right)_{\rho_\mathrm{N}} + \alpha^\mathrm{r} \tag{7}$$

$$= T\left[\sum_{m=2}^{\infty}\frac{1}{m-1}\left(\frac{\partial B_m}{\partial T}\right)\rho_\mathrm{N}^{m-1}\right] + \sum_{m=2}^{\infty}\frac{1}{m-1}B_m(T)\rho_\mathrm{N}^{m-1} \tag{8}$$

$$= T\left[\left(\frac{\partial B_2}{\partial T}\right)\rho_\mathrm{N} + \frac{1}{2}\left(\frac{\partial B_3}{\partial T}\right)\rho_\mathrm{N}^2 + \dots\right] + \left[B_2\rho_\mathrm{N} + \frac{1}{2}B_3\rho_\mathrm{N}^2 + \dots\right] \tag{9}$$

In the limit of $\rho_\mathrm{N} \to 0$, $-s_\mathrm{ex}/k_\mathrm{B}$ goes to zero too. The number density derivative of the excess entropy is equal to

$$\left(\frac{\partial(-s_\mathrm{ex}/k_\mathrm{B})}{\partial \rho_\mathrm{N}}\right)_T = T\left[\sum_{m=2}^{\infty}\left(\frac{\partial B_m}{\partial T}\right)\rho_\mathrm{N}^{m-2}\right] + \sum_{m=2}^{\infty}B_m(T)\rho_\mathrm{N}^{m-2} \tag{10}$$

$$= T\left[\left(\frac{\partial B_2}{\partial T}\right) + \left(\frac{\partial B_3}{\partial T}\right)\rho_\mathrm{N} + \dots\right] + [B_2 + B_3\rho_\mathrm{N} + \dots] \tag{11}$$

and thus in the limit of zero density this derivative is equal to

$$\lim_{\rho_\mathrm{N}\to 0}\left(\frac{\partial(-s_\mathrm{ex}/k_\mathrm{B})}{\partial \rho_\mathrm{N}}\right)_T = T\left(\frac{\partial B_2}{\partial T}\right) + B_2 \tag{12}$$

The temperature derivative of excess entropy is given by

$$\left(\frac{\partial(-s_\mathrm{ex}/k_\mathrm{B})}{\partial T}\right)_{\rho_\mathrm{N}} = T\left(\frac{\partial^2 \alpha^\mathrm{r}}{\partial T^2}\right)_{\rho_\mathrm{N}} + 2\left(\frac{\partial^2 \alpha^\mathrm{r}}{\partial T^2}\right)_{\rho_\mathrm{N}} \tag{13}$$

$$= T\left[\sum_{m=2}^{\infty}\frac{1}{m-1}\left(\frac{\partial^2 B_m}{\partial T^2}\right)\rho_\mathrm{N}^{m-1}\right] + 2\sum_{m=2}^{\infty}\frac{1}{m-1}\left(\frac{\partial^2 B_m}{\partial T^2}\right)\rho_\mathrm{N}^{m-1} \tag{14}$$

$$= T\left[\left(\frac{\partial^2 B_2}{\partial T^2}\right)\rho_\mathrm{N} + \frac{1}{2}\left(\frac{\partial^2 B_3}{\partial T^2}\right)\rho_\mathrm{N}^2 + \dots\right] + \left[2\left(\frac{\partial^2 B_2}{\partial T^2}\right)\rho_\mathrm{N} + \left(\frac{\partial^2 B_3}{\partial T^2}\right)\rho_\mathrm{N}^2 + \dots\right] \tag{15}$$

and the temperature/density cross derivative of excess entropy is given by

$$\left(\frac{\partial^2(-s_\mathrm{ex}/k_\mathrm{B})}{\partial T\partial \rho}\right)_{\rho_\mathrm{N}} = T\left(\frac{\partial^3 \alpha^\mathrm{r}}{\partial T^2\partial \rho_\mathrm{N}}\right) + 2\left(\frac{\partial^3 \alpha^\mathrm{r}}{\partial T^2\partial \rho_\mathrm{N}}\right) \tag{16}$$

$$= T\left[\sum_{m=2}^{\infty}\left(\frac{\partial^2 B_m}{\partial T^2}\right)\rho_\mathrm{N}^{m-2}\right] + 2\sum_{m=2}^{\infty}\left(\frac{\partial B_m}{\partial T}\right)\rho_\mathrm{N}^{m-2} \tag{17}$$

$$= T\left[\left(\frac{\partial^2 B_2}{\partial T^2}\right) + \left(\frac{\partial^2 B_3}{\partial T^2}\right)\rho_\mathrm{N} + \dots\right] + 2\left[\left(\frac{\partial B_2}{\partial T}\right) + \left(\frac{\partial B_3}{\partial T}\right)\rho_\mathrm{N} + \dots\right] \tag{18}$$

1.2 Dilute gas limit

To begin we consider the scaled viscosity and its dilute-gas limit

$$\lim_{\rho_\mathrm{N}\to 0} \eta^+ = \frac{\eta}{\sqrt{mk_\mathrm{B}T}} \frac{0^{2/3}}{0^{2/3}} \tag{19}$$

We want the dilute gas limit of this term, so we define a new proxy variable

$$\eta^\bullet \equiv \left(\frac{\eta^+ \sqrt{mk_\mathrm{B}T}}{\eta} \right)^{3/2} = \frac{-s_\mathrm{ex}/k_\mathrm{B}}{\rho_\mathrm{N}} \tag{20}$$

and take its zero-density limit

$$\lim_{\rho_\mathrm{N}\to 0} \eta^\bullet = \lim_{\rho_\mathrm{N}\to 0} \frac{-s_\mathrm{ex}/k_\mathrm{B}}{\rho_\mathrm{N}} = \frac{0}{0}. \tag{21}$$

Still indeterminate... Application of l'Hôpital's rule to this indeterminate form and substitution of Eq. (12) yields

$$\lim_{\rho_\mathrm{N}\to 0} \eta^\bullet = \lim_{\rho_\mathrm{N}\to 0} \frac{\left(\frac{\partial(-s_\mathrm{ex}/k_\mathrm{B})}{\partial \rho_\mathrm{N}} \right)_T}{\cancelto{1}{\left(\frac{\partial \rho_\mathrm{N}}{\partial \rho_\mathrm{N}} \right)}} = \lim_{\rho_\mathrm{N}\to 0} \left(\frac{\partial(-s_\mathrm{ex}/k_\mathrm{B})}{\partial \rho_\mathrm{N}} \right)_T = T \left(\frac{\partial B_2}{\partial T} \right) + B_2 \tag{22}$$

The dilute gas limit of η^+ is equal to

$$\lim_{\rho\to 0} \eta^+ = \frac{\eta_{\rho_\mathrm{N}\to 0}}{\sqrt{mk_\mathrm{B}T}} \left(\lim_{\rho_\mathrm{N}\to 0} \eta^\bullet \right)^{2/3} = \frac{\eta_{\rho_\mathrm{N}\to 0}}{\sqrt{mk_\mathrm{B}T}} \left[T \left(\frac{\partial B_2}{\partial T} \right) + B_2 \right]^{2/3} \tag{23}$$

$$\lim_{\rho\to 0} \left(\frac{\partial(-s_\mathrm{ex}/k_\mathrm{B})}{\partial \rho_\mathrm{N}} \right)_T = T \left(\frac{\mathrm{d}B_2}{\mathrm{d}T} \right) + B_2, \tag{24}$$

resulting in

$$\lim_{\rho_\mathrm{N}\to 0} \eta^+ = \frac{\eta_{\rho_\mathrm{N}\to 0}}{\sqrt{mk_\mathrm{B}T}} \left[T \left(\frac{\mathrm{d}B_2}{\mathrm{d}T} \right) + B_2 \right]^{2/3} \tag{25}$$

$$= \frac{\eta^*_{\rho\to 0}}{\sqrt{T^*}} \left[T^* \left(\frac{\mathrm{d}B_2^*}{\mathrm{d}T^*} \right) + B_2^* \right]^{2/3}. \tag{26}$$

The approach for thermal conductivity and self-diffusion is analogous, resulting in

$$\lim_{\rho_\mathrm{N}\to 0} \lambda^+ = \frac{\lambda_{\rho_\mathrm{N}\to 0}}{k_\mathrm{B}\sqrt{k_\mathrm{B}T/m}} \left[T\left(\frac{\mathrm{d}B_2}{\mathrm{d}T}\right) + B_2\right]^{2/3} \tag{27}$$

$$= \frac{\lambda^*_{\rho_\mathrm{N}\to 0}}{\sqrt{T^*}} \left[T^*\left(\frac{\mathrm{d}B_2^*}{\mathrm{d}T}\right) + B_2^*\right]^{2/3} \tag{28}$$

In the case of self-diffusion, the product of density and self-diffusion is considered, rather than the self-diffusion alone because the product $\rho_\mathrm{N} D$ (or equivalently $\rho^* D^*$) is finite at zero density. Therefore the mathematical approach for the self-diffusion is analogous, resulting in

$$\lim_{\rho_\mathrm{N}\to 0} D^+ = \frac{(\rho_\mathrm{N} D)_{\rho_\mathrm{N}\to 0}}{\sqrt{k_\mathrm{B}T/m}} \left[T\left(\frac{\mathrm{d}B_2}{\mathrm{d}T}\right) + B_2\right]^{2/3} \tag{29}$$

$$= \frac{(\rho^* D^*)_{\rho_\mathrm{N}\to 0}}{\sqrt{T^*}} \left[T^*\left(\frac{\mathrm{d}B_2^*}{\mathrm{d}T^*}\right) + B_2^*\right]^{2/3} . \tag{30}$$

1.3 2/3 is Special

Suppose that we are interested in a power of residual entropy in η^+ other than 2/3, in this case with the exponent w. To begin we consider the scaled viscosity

$$\eta^{w+} = \frac{\eta}{\rho_\mathrm{N}^{2/3}\sqrt{mk_\mathrm{B}T}} \left(-s^\mathrm{r}/R\right)^w . \tag{31}$$

We want the dilute gas limit of η^{w+}, so we define a new proxy variable

$$\eta^{\bullet\bullet} \equiv \left(\frac{\eta^{w+}\sqrt{mk_\mathrm{B}T}}{\eta}\right)^{3/2} = \frac{\left(-s_\mathrm{ex}/k_\mathrm{B}\right)^{\frac{3w}{2}}}{\rho_\mathrm{N}} \tag{32}$$

And as before, apply l'Hôpital's rule to the indeterminate limit

$$\lim_{\rho_\mathrm{N}\to 0} \eta^{\bullet\bullet} = \lim_{\rho_\mathrm{N}\to 0} \frac{\frac{3w}{2}\left(-s_\mathrm{ex}/k_\mathrm{B}\right)^{\frac{3w}{2}-1}\left(\frac{\partial(-s_\mathrm{ex}/k_\mathrm{B})}{\partial\rho}\right)_T}{\cancelto{1}{\left(\frac{\partial\rho}{\partial\rho}\right)}} = \lim_{\rho_\mathrm{N}\to 0} \frac{3w}{2}\left(-s_\mathrm{ex}/k_\mathrm{B}\right)^{\frac{3w}{2}-1}\left(\frac{\partial(-s_\mathrm{ex}/k_\mathrm{B})}{\partial\rho}\right)_T \tag{33}$$

This limit will be identically equal to zero if $(3w/2) - 1$ is any value other than zero; $0^0 = 1$. In order to make $(3w)/2 - 1$ equal zero, w must be equal to 2/3 to have a finite value of the limit at zero density. The exponent of 2/3 is indeed special, and the only value that can be used.

1.4 Dilute Gas Correction Terms

In Kim and Monroe,[S1] the collision integrals were all obtained with empirical forms equal to

$$\Omega^{(l,s)*} = A^{(l,s)} + \sum_{k=1}^{6} \left[\frac{B_k^{(l,s)}}{(T^*)^k} + C_k^{(l,s)} (\ln(T^*))^k \right] \tag{34}$$

The higher-order correction terms $f_\eta^{(3)}$, $f_\lambda^{(3)}$, $f_D^{(2)}$ are obtained from Equations 31 to 36 of Kim and Monroe. Implementations of the higher-order correction terms, as well as all the necessary coefficients, are included in the Python file `implementation.py`.

1.5 Critical Enhancement to Conductivity

In engineering units, Olchowy and Sengers[S2] gives the critical enhancement

$$\Delta_\mathrm{c}\lambda = \frac{R_\mathrm{D}}{6\pi} \frac{\rho_\mathrm{N} c_\mathrm{p,N} k_\mathrm{B} T}{\eta \xi} (\Omega - \Omega_0) \tag{35}$$

$$\Omega = \frac{2}{\pi} \left[(1 - \kappa^{-1}) \arctan(y) + \kappa^{-1} y \right] \tag{36}$$

$$\Omega_0 = \frac{2}{\pi} \left[1 - \exp\left(-\frac{1}{y^{-1} + (y/\delta)^2/3} \right) \right] \tag{37}$$

with $\kappa = c_p/c_v$, $y = \xi/(q_\mathrm{D}^{-1})$, $\delta = \rho/\rho_\mathrm{c}$.

$$\xi = \xi_0 \left(\frac{p_\mathrm{c} \rho_\mathrm{N}}{\Gamma \rho_\mathrm{c,N}^2} \right)^{\nu_\lambda/\gamma_\lambda} \left[\left(\frac{\partial \rho_\mathrm{N}(T, \rho_\mathrm{N})}{\partial p} \right)_T - \frac{T_\mathrm{R}}{T} \left(\frac{\partial \rho_\mathrm{N}(T_\mathrm{R}, \rho_\mathrm{N})}{\partial p} \right)_T \right]^{\nu_\lambda/\gamma_\lambda} \tag{38}$$

Defining new reduced variables $\xi^* = \xi/\sigma$, $\xi_0^* = \xi_0/\sigma$, substitution and cancellation results in

$$\xi^* = \xi_0^* \left(\frac{p_\mathrm{c}^* \rho^*}{\Gamma (\rho_\mathrm{c}^*)^2} \right)^{\nu_\lambda/\gamma_\lambda} \left[\left(\frac{\partial \rho^*(T^*, \rho^*)}{\partial p^*} \right)_{T^*} - \frac{T_\mathrm{R}^*}{T^*} \left(\frac{\partial \rho^*(T_\mathrm{R}^*, \rho^*)}{\partial p^*} \right)_{T^*} \right]^{\nu_\lambda/\gamma_\lambda} \tag{39}$$

And the critical enhancement contribution is a bit more complicated:

$$\frac{\Delta_\mathrm{c}\lambda^* k_\mathrm{B} \sqrt{\varepsilon/m}}{\sigma^2} = \frac{R_\mathrm{D}}{6\pi} \frac{\frac{\rho^*}{\sigma^3} (k_\mathrm{B} c_p^*)(T^* \varepsilon)}{\left(\frac{\eta^* \sqrt{\varepsilon m}}{\sigma^2} \right) \xi^* \sigma} (\Omega - \Omega_0) \tag{40}$$

yielding

$$\Delta_\mathrm{c}\lambda^* = \frac{R_\mathrm{D}}{6\pi} \frac{\rho^* c_p^* T^*}{\eta^* \xi^*} (\Omega - \Omega_0) \tag{41}$$

and $y = \xi^*/(q_\mathrm{D}^{-1})^*$

2 Data Analysis

2.1 Data Tables

Table S1: Literature data for self-diffusivity. Values reported in parentheses apply to only a small subset of the data.

Author	Year	N_d	T^*	ρ^*	Method	Ensemble	TS	N	r^*_{cut}	t^*_{eq}	t^*_{prod}	δt^*
Baidakov[S3]	2011	198	0.35-2	0.005-1.2	EMD, ER/GK	NVE	–	2048	5.975-6.78, LRTC	1050-1610	2300-57500	(0.0023), 0.0046
Borgelt[S4]	1990	46	0.664-2.715	0.781-0.884	EMD, GK	NVE	–	108	2.5	–	371.2	0.00464
Costigliola[S5]	2018	362	0.8-10793.4	0.316-3.39	EMD, ER	NVT	NH	1000	2.5, LJTS		500000	0.001
Hammonds[S6]	1988	51	0.72-10	0.4-1.18	EMD, GK	(NVE), NVT	GI	(108), 256, 500	–	–	(14000), 3000-4000	0.015-0.02
Heyes[S7]	1983	54	0.68-4.58	0.2-1.113	EMD, ER	–	–	256	2.5, LRTC	–	150-300	0.0025, 0.005
Heyes[S8]	1988	212	0.72-10	0.2-1.22	EMD, GK	–	–	108, 256, 500	–	–	(3300-8800)$\times\rho^* T^{*\frac{-1}{2}}$	0.022 $\rho^* T^{*\frac{-1}{2}}$
Heyes[S9]	1990	26	0.722-6	0.4-1.4	EMD, GK	NVT	VR	256	2.5	–	1500	0.015
Lautenschlaeger[S10]	2019	186	0.7019-10.01	0.20134-1.1954	NEMD, 2G-G	–	GI	10,000	2.5, LJTS	1,000	4,000	0.002
Lautenschlaeger[S10]	2019	159	0.65919-4.3379	0.22223-0.93754	NEMD, 2G-L	–	GI	10,000	2.5, LJTS	1,000	4,000	0.002
Meier[S11]	2004	334	0.698757-6.004	0.005-1.275	EMD, ER	NVE	–	256, 500, 864, 1372	5.5-6.5	300-900	4500-6000	0.003
Michels[S12]	1978	43	1.3-5.56	0.01-0.3024	EMD, GK	NVT	VR	125	2.5, LJTS		300-25300	0.005
Oderji[S13]	2011	152	0.6964-30.1953	0.0005-0.05	EMD, GK/ER	NVE	–	2048	6.75	2300-11500	115000-230000	0.0023
Rowley[S14]	1997	171	0.8-4	0.05-1	EMD, ER	NVT	–	256	4	150	540-6000	(0.001), 0.003
Straub[S15]	1992	35	0.75-4	0.3-1.05	EMD, ER	–	–	512	2.5	50	150	0.001

Table S2: Literature data for thermal conductivity. Values reported in parentheses apply to only a small subset of the data.

Author	Year	N_d	T^*	ρ^*	Method	Ensemble	TS	N	r^*_{cut}	t^*_{eq}	t^*_{prod}	δt^*
Baidakov[S16]	2014	235	0.4-2	0.01-1.2	EMD, GK	NVE	–	4000	6.78, LRTC	230	13800	0.0023
Borgelt[S4]	1990	46	0.664-2.715	0.781-0.884	EMD, GK	NVE	–	108	2.5		371.2	0.00464
Bugel[S17]	2008	102	0.6-4	0.25-0.9	NEMD, BHE	–	Bn	1500	2.5	200	1000	0.002
Galliero[S18]	2009	36	0.8-8	0.1-1	NEMD, RP	–	Bn	3000	2.5		30000	0.003
Hammonds[S6]	1988	50	0.72-10	0.4-1.18	EMD, GK	(NVE), NVT	GI	(108), 256, 500	–	–	3000-4000 (14000)	0.015-0.02
Heyes[S8]	1988	213	0.72-10	0.2-1.22	EMD, GK	–	–	108, 256, 500	–	–	$(3300\text{-}8800)\times\rho^* T^{*\frac{-1}{2}}$	$0.022\times\rho^* T^{*\frac{-1}{2}}$
Heyes[S8]	1988	8	1.95-2	0.3-1.04	NEMD, H	–	–	256, 2048	–	–	$(440\text{-}1760)\times\rho^* T^{*\frac{-1}{2}}$	$0.022\times\rho^* T^{*\frac{-1}{2}}$
Heyes[S9]	1990	26	0.722-6	0.4-1.4	EMD, GK	NVT	VR	256	2.5		1500	0.015
Hoheisel[S19]	1990	14	0.745-3.564	0.65-0.85	EMD, GK	NVE	–	(108-2048), 256	2.5		464	0.00464
Lautenschlaeger[S10]	2019	186	0.7019-10.01	0.20134-1.1954	NEMD, 2G-G	–	GI	10,000	2.5, LJTS	1,000	4,000	0.002
Lautenschlaeger[S10]	2019	159	0.65919-4.3379	0.22223-0.93754	NEMD, 2G-L	–	GI	10,000	2.5, LJTS	1,000	4,000	0.002
Levesque[S20]	1987	9	0.733-2.725	0.844-0.962	EMD, GK	–	–	108, 256, 864	–	111-891		0.00464
Meier[S21]	2002	31	1.3458-1.3588	0.05-0.95	EMD, GK/ER	NVE	–	1372	5.5	300-900	6000-30000	0.003
Mountain[S22]	2006	14	0.745-3.564	0.65-0.85	NEMD, RP	–	NH	250	3	1000	10,000	0.0025
Nasrabad[S23]	2006	67	0.9-2	0.2-0.9	EMD, GK	NVT	Bn	864	4	250	10000-20000	0.005
Vogelsang[S24]	1987	3	0.94-1.27	0.65-0.715	EMD, GK	–	–	(32-1372), 108	(1.6-3.5), 2.25	(232-928), 464		0.00464
Vogelsang[S25]	1988	14	0.745-3.564	0.65-0.85	EMD, GK	NVE	–	(108), 256	2.5	464		0.00464

Table S3: Literature data for shear viscosity. Values reported in parentheses apply to only a small subset of the data.

Author	Year	N_d	T^*	ρ^*	Method	Ensemble	TS	N	r^*_{cut}	t^*_{eq}	t^*_{prod}	δt^*
Baidakov[S26]	2012	216	0.4-2	0.01-1.2	EMD, GK	NVE	–	4000	6.78, LRTC	575-805	13800, 27600	0.0023
Borgelt[S4]	1990	46	0.664-2.715	0.781-0.884	EMD, GK	NVE	–	108	2.5	–	371.2	0.00464
Costigliola[S5]	2018	362	0.8-10793.4	0.316-3.39	NEMD, SLLOD	–	GI	1000	2.5, LJTS	500000		0.001
Galliero[S27]	2005	80	0.6-4	0.212-1	NEMD, RP	NVT	Bn	1500	2.5	20000		0.002
Gosling[S28]	1973	3	0.937-1.162	0.625-0.801	EMD, GK	–	–	256	–	464		0.00464
Hammonds[S6]	1988	51	0.72-10	0.4-1.18	EMD, GK	(NVE), NVT	GI	(108), 256, 500	–	–	3000-4000 (14000)	0.015-0.02
Heyes[S7]	1983	52	0.68-4.58	0.2-1.113	NEMD	–	–	256	2.5, LRTC	–	150-300	0.0025, 0.005
Heyes[S8]	1988	210	0.72-10	0.2-1.22	EMD, GK	–	–	108, 256, 500	–	–	(3300-8800)$\times\rho^*T^{*\frac{-1}{2}}$	0.022$\times\rho^*T^{*\frac{-1}{2}}$
Heyes[S8]	1988	87	0.72-10	0.2-1.22	NEMD, SLLOD	–	–	256, 2048	–	–	(440-1760)$\times\rho^*T^{*\frac{-1}{2}}$	0.022$\times\rho^*T^{*\frac{-1}{2}}$
Heyes[S9]	1990	26	0.722-6	0.4-1.4	EMD, GK	NVT	VR	256	2.5	–	1500	0.015
Hoheisel[S19]	1990	3	0.73-2.47	0.844-1	EMD, GK/TCAF	NVE	–	(108-2048), 256	2.5	–	464	0.00464
Lautenschlaeger[S10]	2019	186	0.7019-10.01	0.20134-1.1954	NEMD, 2G-G	–	GI	10,000	2.5, LJTS	1,000	4,000	0.002
Lautenschlaeger[S10]	2019	159	0.65919-4.3379	0.22223-0.93754	NEMD, 2G-L	–	GI	10,000	2.5, LJTS	1,000	4,000	0.002
Levesque[S20]	1987	9	0.733-2.725	0.844-0.962	EMD, GK	–	–	108, 256, 864	–	111-891		0.00464
Meier[S29]	2004	402	0.698757-6.004	0.005-1.275	EMD, ER	NVE	–	(108-4000), 1372	(2.5-5.5), 5-6.5	300-900	4500-6000 (30,000-150,000)	0.003
Michels[S30]	1985	36	1.3-10	0.05-0.3	EMD, GK	–	–	108	2.5	(8000-48000)$\times T^{*\frac{-1}{2}}$		0.004$\times T^{*\frac{-1}{2}}$
Mountain[S22]	2006	14	0.745-3.564	0.65-0.85	NEMD, RP	NVT	NH	250	3	1000	10,000	0.0025
Oderji[S13]	2011	154	0.6964-30.1953	0.0005-0.05	EMD, GK/ER	NVE	–	2048	6.75	2300-11500	115000-230000	0.0023
Rowley[S14]	1997	116	0.8-4	0.05-1	EMD, ER	NVT	–	256	4	150	540-6000	(0.001), 0.003
Schoen[S31]	1985	14	0.94-4.42	0.4005-1.113	EMD, GK	–	–	(32-2048), 500	2.5	2.784	464	0.00464
Vasquez[S32]	2004	104	0.7-6.003	0.05-1.3	NEMD, SSPP	NVT	NH	1000	5, LJTS	2000		0.005
Vogelsang[S25]	1988	14	0.745-3.564	0.65-0.85	EMD, GK	NVE	–	(108), 256	2.5	464		0.00464

Table S4: Nomenclature for Tables S1, S2, and S3.

Notation	Description
2G	Two-gradient (NEMD)[S33]
2G-G	Global two-gradient (NEMD)[S33]
2G-L	Local two-gradient (NEMD)[S33]
BHE	Boundary heat exchange (NEMD)[S34]
Bn	Berendsen thermostat[S35]
δt^*	Time-step (reduced LJ units)
EMD	Equilibrium molecular dynamics
ER	Einstein relation (EMD)
GI	Gaussian isokinetic thermostat[S36]
GK	Green-Kubo (EMD)
H	Homogenous (NEMD)[S37,S38]
LJTS	Lennard-Jones truncated-and-shifted
LRTC	Long-range tail corrections
N	Number of particles
$\mathrm{N_d}$	Number of data points
NEMD	Non-equilibrium molecular dynamics[S39]
NH	Nosé-Hoover thermostat[S40,S41]
NVE	Constant number of molecules, volume, and energy
NVT	Constant number of molecules, volume, and temperature
r^*_{cut}	Cut-off distance (reduced LJ units)
RP	Reverse perturbation (NEMD)[S42–S45]
SLLOD	Homogenous planar shear equations of motion (NEMD)[S46,S47]
SSPP	Steady-state periodic perturbation NEMD[S28]
t^*_{eq}	Equilibration time (reduced LJ units)
t^*_{prod}	Production time (reduced LJ units)
TCAF	Transverse autocorrelation function (EMD)[S48]
TS	Thermostat
VR	(Canonical sampling) velocity rescaling thermostat[S49]

3 Larger figures

3.1 Rosenfeld scaling

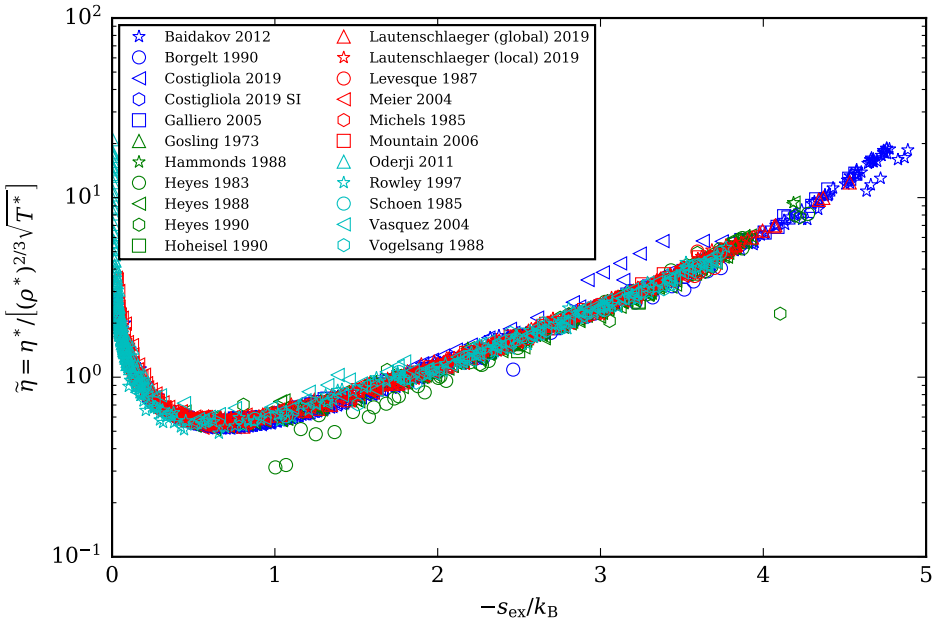

Figure S1: Rosenfeld-scaled viscosity values from simulations[S4,S6–S10,S10,S13,S14,S19,S20,S22,S25–S32,S50,S51] for the Lennard-Jones 12-6 potential.

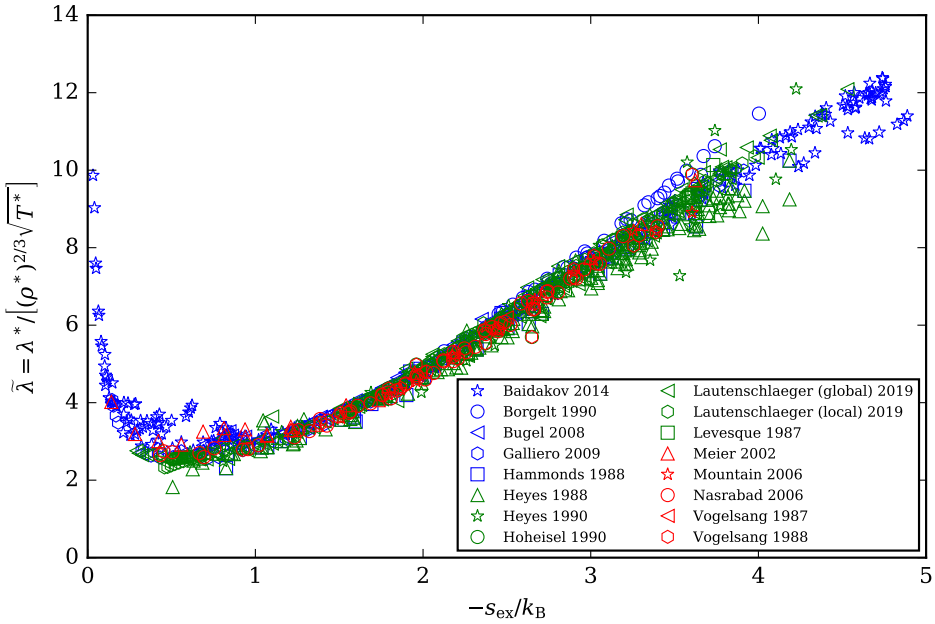

Figure S2: Rosenfeld-scaled thermal conductivity values from simulations[S4,S6,S8–S10,S10,S16–S25] for the Lennard-Jones 12-6 potential.

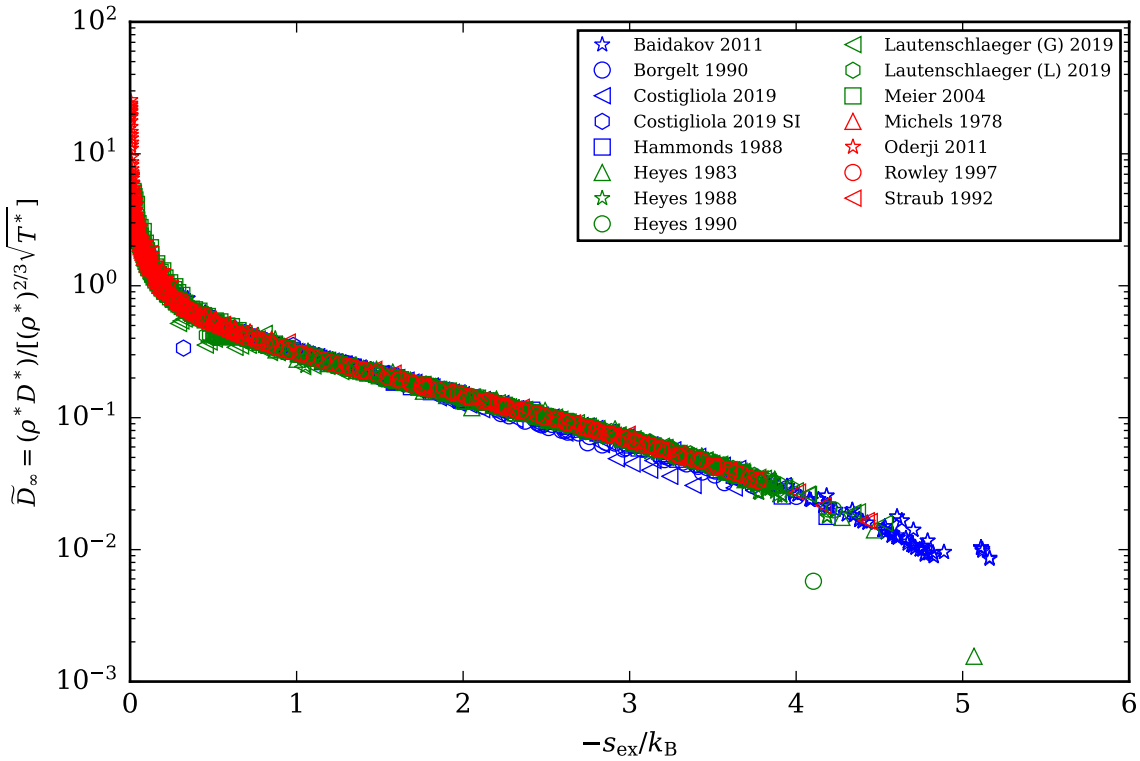

Figure S3: Rosenfeld-scaled self-diffusion values from simulations[S3,S4,S6–S10,S10–S15,S50,S51] for the Lennard-Jones 12-6 potential.

3.2 Novel scaling

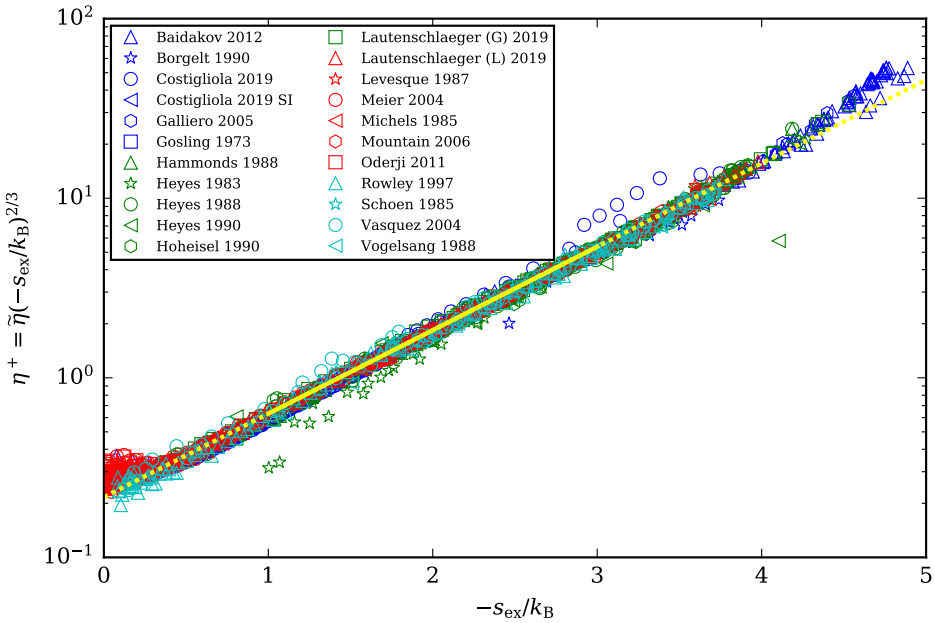

Figure S4: Overview of all of the novel scaled viscosity data from simulations[S4,S6–S10,S10,S13,S14,S19,S20,S22,S25–S32,S50,S51] for the Lennard-Jones 12-6 potential. The yellow curve is the fitted correlation.

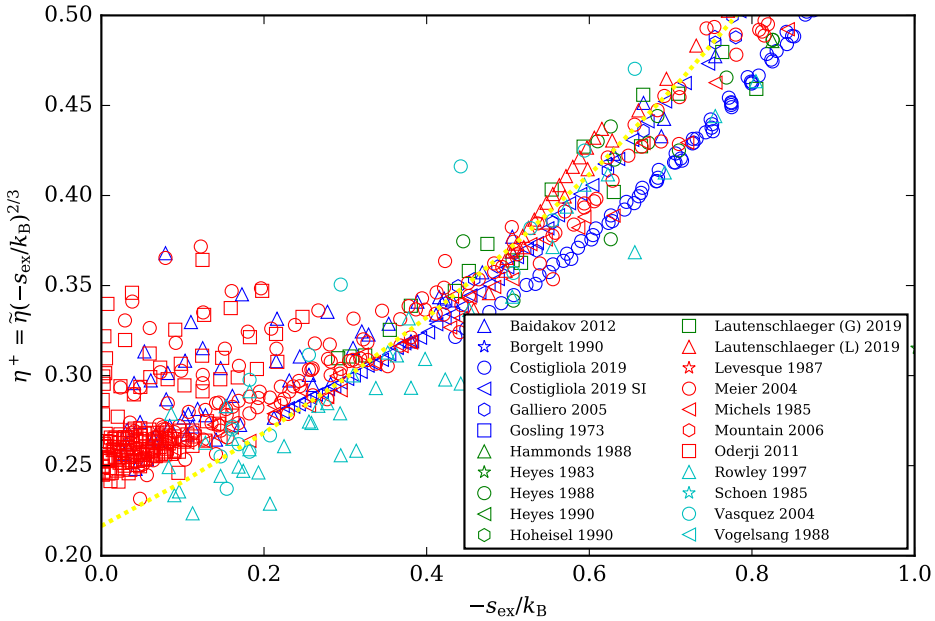

Figure S5: Detailed view of the gaseous region of the novel scaled viscosity data from simulations for the Lennard-Jones 12-6 potential.

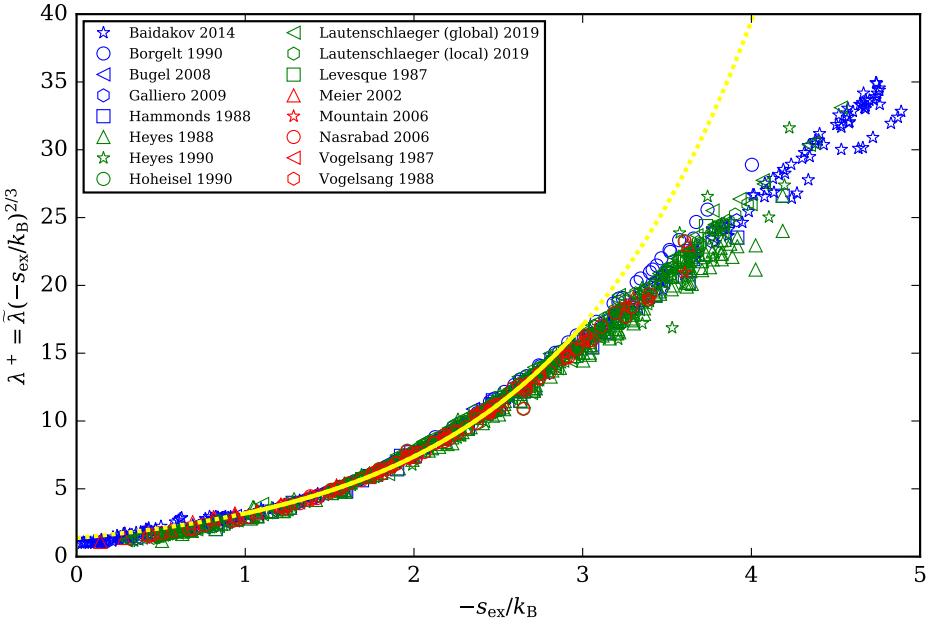

Figure S6: Overview of all the novel scaled thermal conductivity data[S4,S6,S8–S10,S10,S16–S25] from simulations for the Lennard-Jones 12-6 potential. The yellow curve is the fitted correlation.

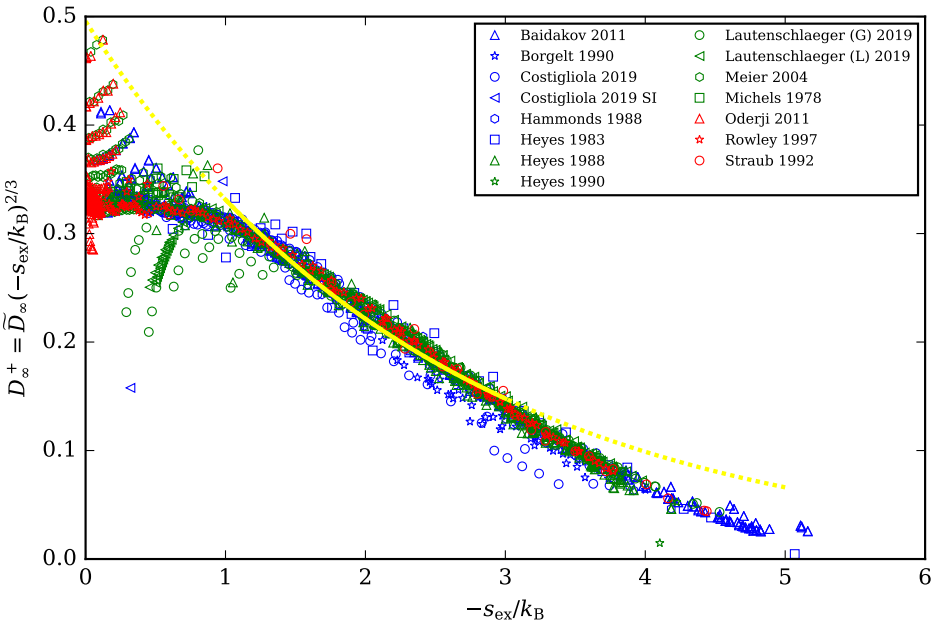

Figure S7: Overview of all the novel scaled self-diffusion[S3,S4,S6–S10,S10–S15,S50,S51] data from simulations for the Lennard-Jones 12-6 potential. The yellow curve is the fitted correlation.

3.3 Uncertainty in D

The uncertainty in D^*_∞, considering the uncertainty in η^* and D^*_N is given by

$$u(D^*_\infty) = \sqrt{\left(\frac{\partial D^*_\infty}{\partial D^*_N}\right)^2 u(D^*_N)^2 + \left(\frac{\partial D^*_\infty}{\partial \eta^*}\right)^2 u(\eta^*)^2} \tag{42}$$

where

$$\left(\frac{\partial D^*_\infty}{\partial D^*_N}\right) = 1 \tag{43}$$

$$\left(\frac{\partial D^*_\infty}{\partial \eta^*}\right) = \frac{T^*\mathfrak{X}}{6\pi L^*}\frac{-1}{(\eta^*)^2} \tag{44}$$

We take constant and conservative absolute uncertainties of

$$u(D^*_N) = 0.01 D^*_N \tag{45}$$

$$u(\eta^*) = 0.1\eta^* \tag{46}$$

3.4 Data plots

In the following subsections, plots are provided for each of the datasets, and for each temperature that appears in the dataset, the value in the zero-density-limit is plotted with a star. These figures allow for a sense of the coverage of each of the individual datasets, and to see graphically whether the data are consistent with the zero-density-limit. The figures are small, and intended to be viewed on the computer zoomed in.

3.4.1 Thermal Conductivity

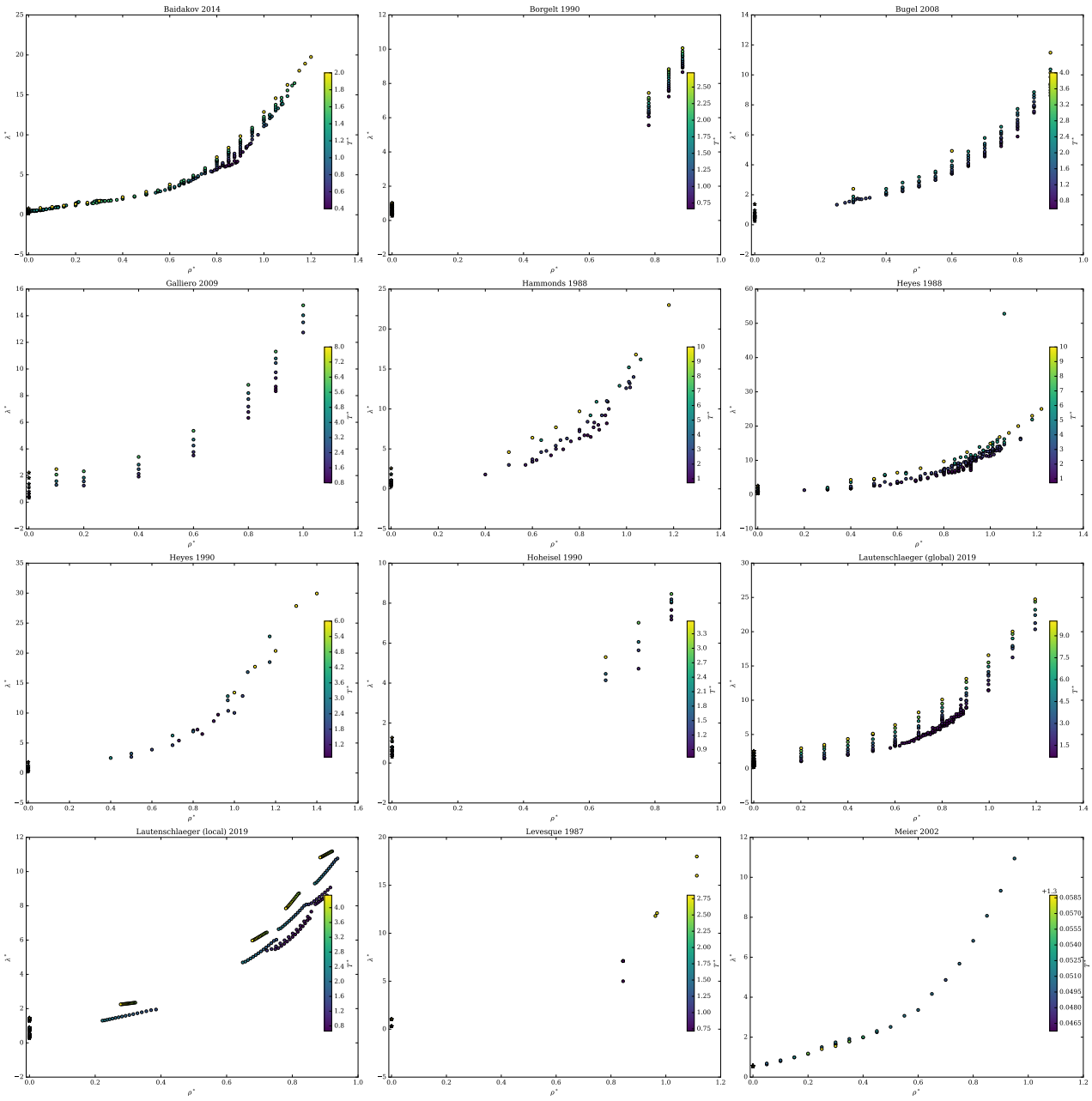

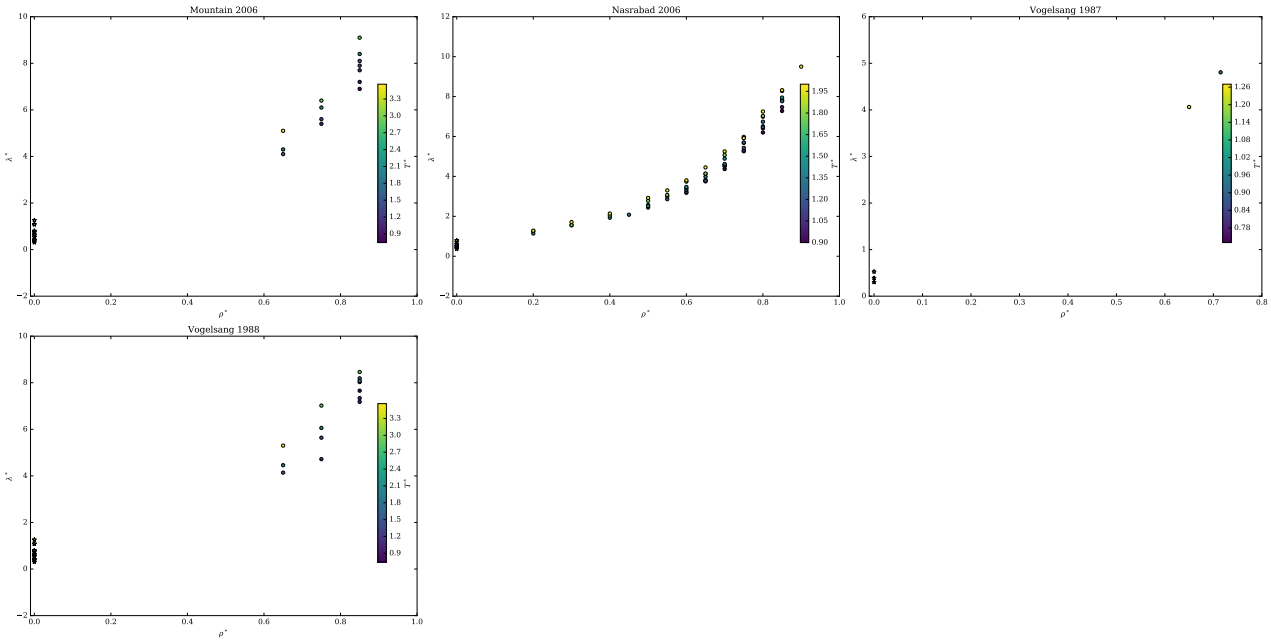

3.4.2 Self-Diffusion

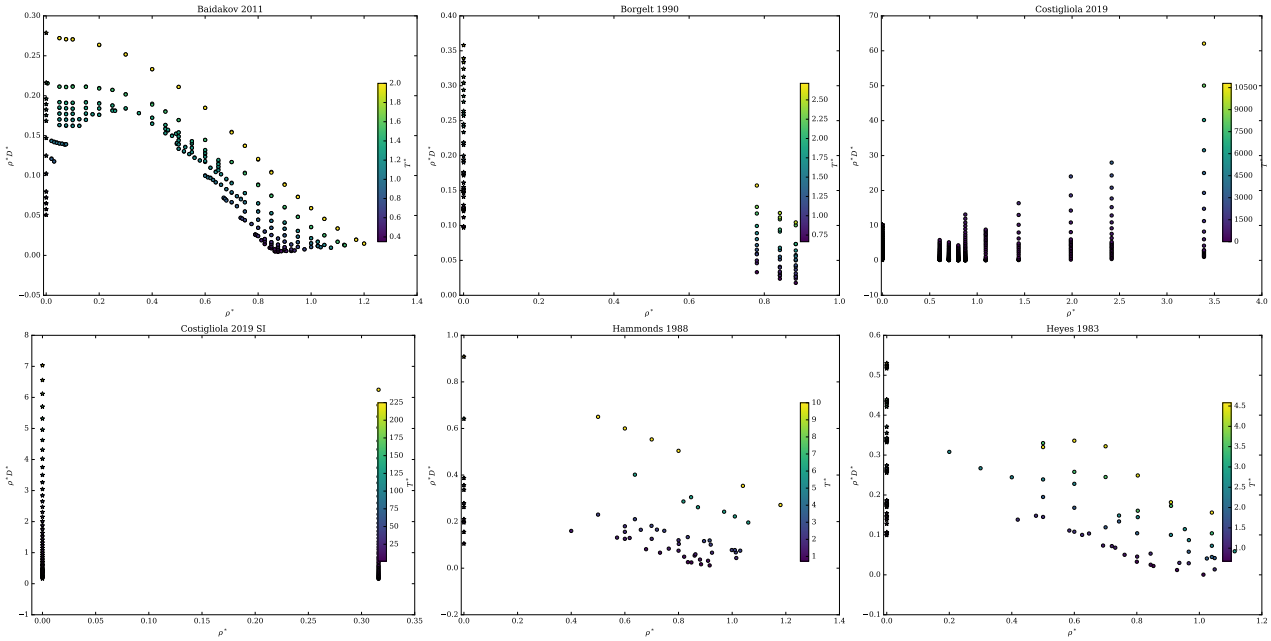

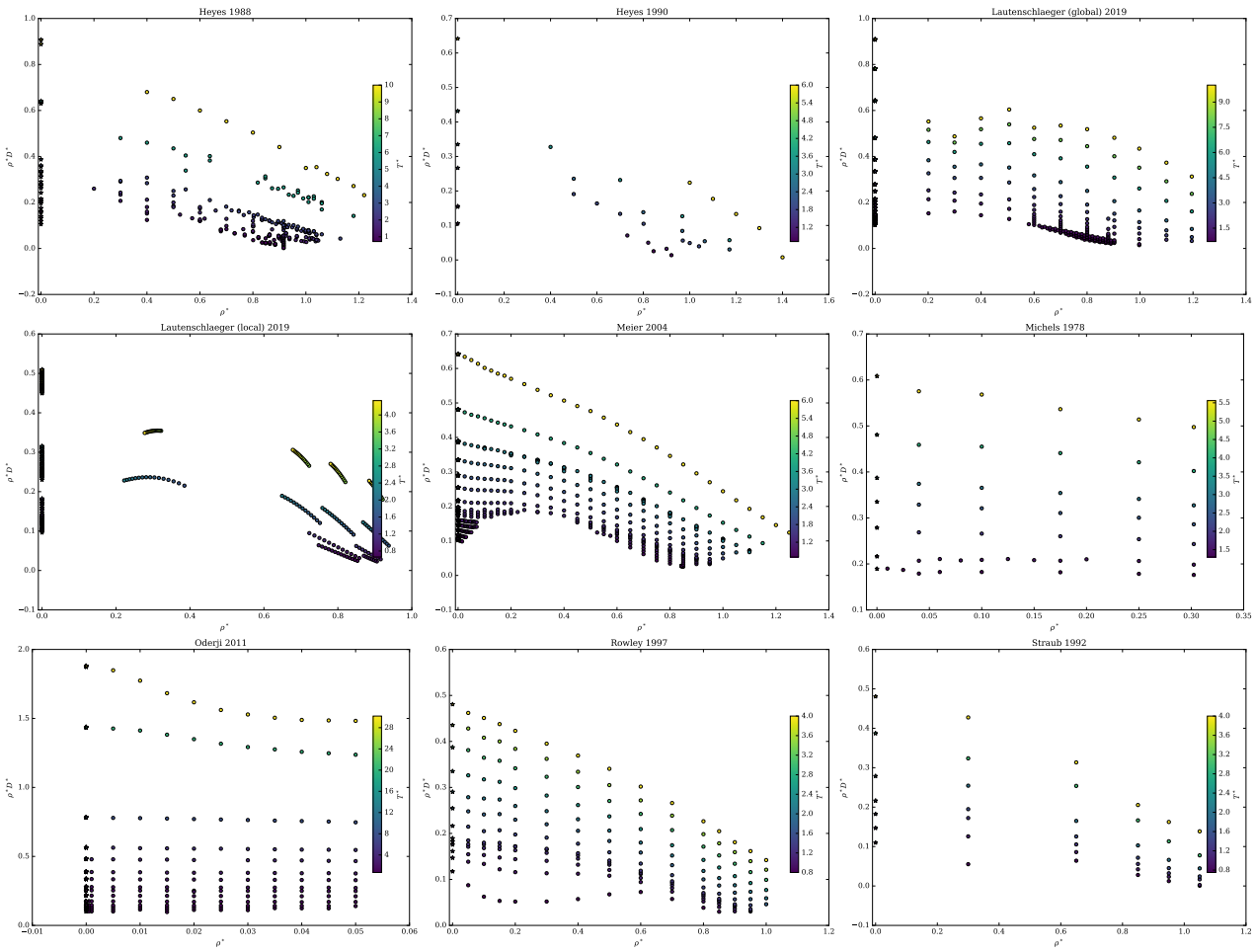
Heyes 1988
Heyes 1990
Lautenschlaeger (global) 2019
Lautenschlaeger (local) 2019
Meier 2004
Michels 1978
Oderji 2011
Rowley 1997
Straub 1992
$\rho^* D^*$
ρ^*
T^*

3.4.3 Viscosity

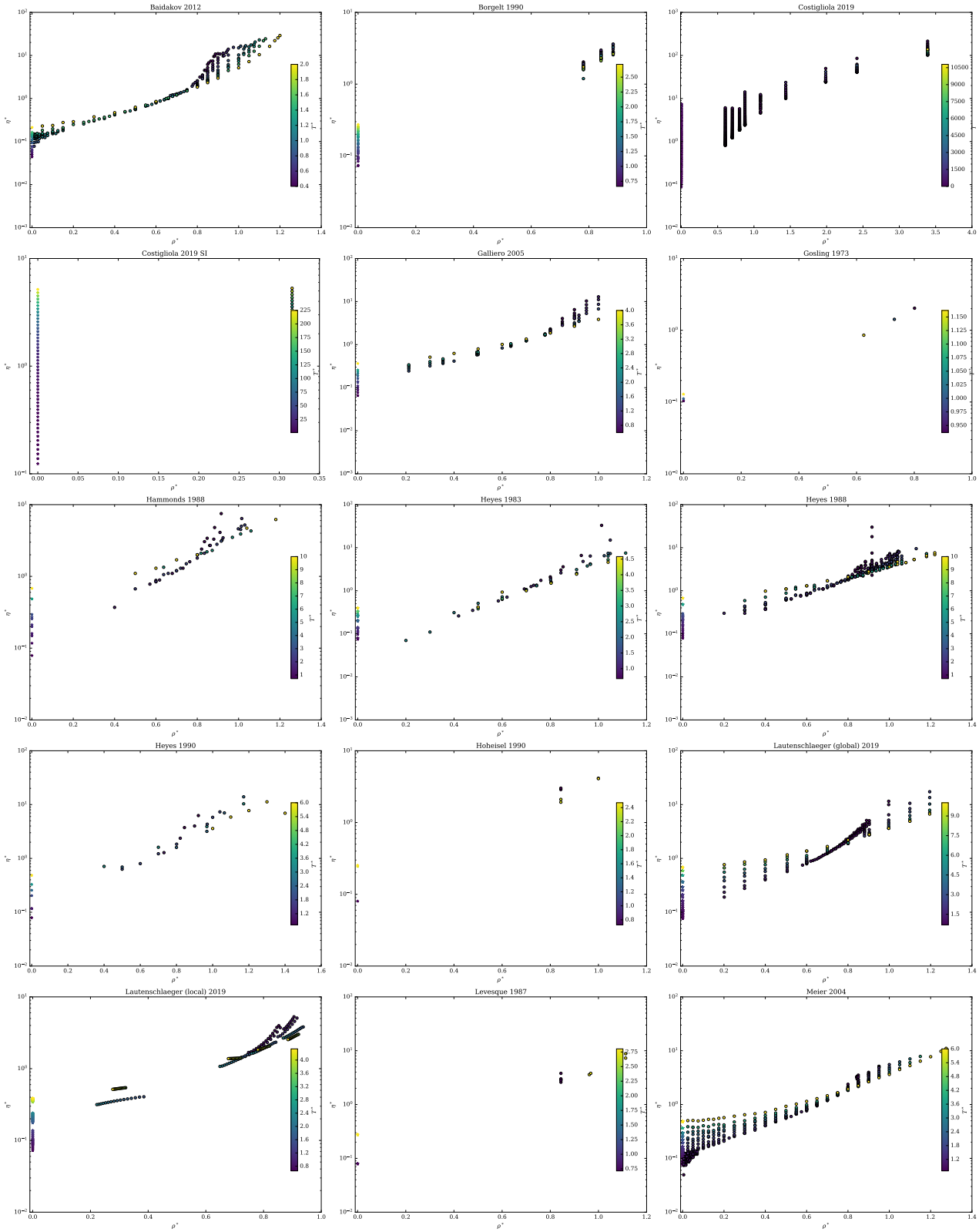

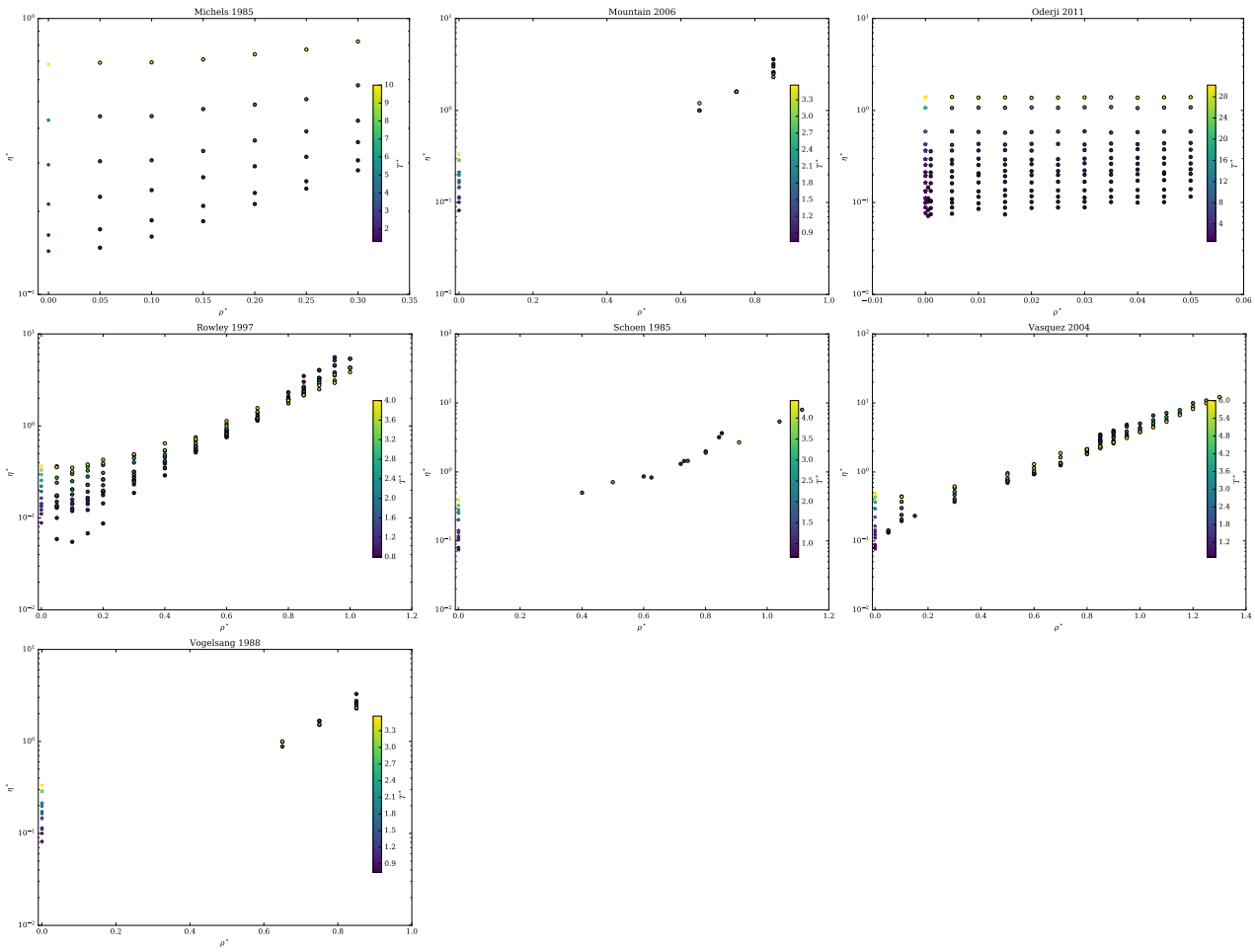
Michels 1985
Mountain 2006
Oderji 2011
Rowley 1997
Schoen 1985
Vasquez 2004
Vogelsang 1988
η^*
ρ^*
T^*

3.5 Correction term of Yeh and Hummer

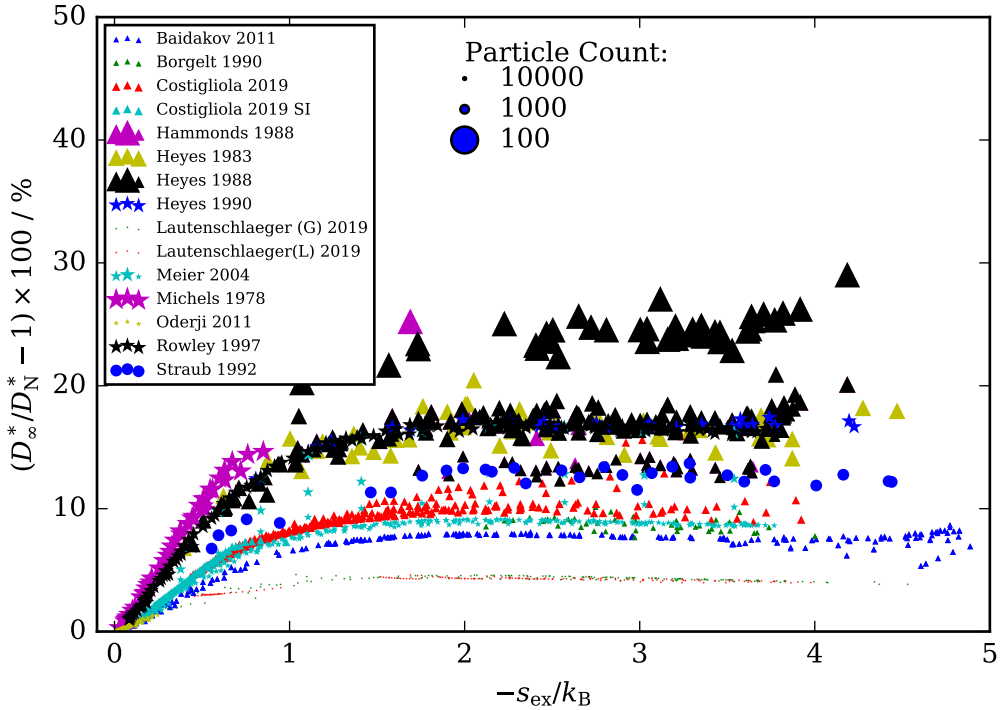

Figure S8: The relative correction to self-diffusion data obtained from the correction term of Yeh and Hummer[S52]

4 Inverse Power Law Potential

Inverse-power-law (IPL) potentials of the form $U = \varepsilon(r/\sigma)^{-n} = (\varepsilon\sigma^n)/r^n$ are another commonly considered intermolecular potential.

4.1 Thermodynamics

From Barlow[S53]

$$B_2 = \bar{B}_2\sigma^3(T^*)^{-3/n}, \tag{47}$$

Sherwood and Mason[S55] and Barlow et al.[S53] give closed form solutions for $\bar{B}_2$ for IPL:

$$\bar{B}_2 = \frac{2\pi}{3}\Gamma(1-3/n) \tag{48}$$

where Γ is the mathematical gamma function. The scaled second virial coefficient is given by

$$B_2^* = \frac{B_2}{\sigma^3}, \tag{49}$$

therefore

$$B_2^* = \bar{B}_2(T^*)^{-3/n} \tag{50}$$

The derivative is given by

$$T^*\left(\frac{\partial B_2^*}{\partial T^*}\right) = \bar{B}_2(-3/n)(T^*)^{-3/n}, \tag{51}$$

With the sum

$$T^*\left(\frac{\partial B_2^*}{\partial T^*}\right) + B_2^* = \bar{B}_2(1-3/n)(T^*)^{-3/n} = \bar{B}_2(1-3/n)(T^*)^{-3/n}, \tag{52}$$

and therefore

$$\left(T^*\left(\frac{\partial B_2^*}{\partial T^*}\right) + B_2^*\right)^{2/3} = (\bar{B}_2(1-3/n))^{2/3}(T^*)^{-2/n}. \tag{53}$$

4.2 Derivations of IPL hardness terms

The formulation of Hirschfelder,[S57] with the variable transformation $d = \varepsilon\sigma^n$, yields

$$\eta = \frac{\frac{5}{8}\sqrt{\frac{k_\mathrm{B}m}{\pi}}\left(\frac{k_\mathrm{B}}{n\varepsilon\sigma^n}\right)^{2/n}T^{\frac{1}{2}+\frac{2}{n}}}{\Gamma(4-\frac{2}{n})A_2(\nu=n+1)/2^{2/n}} \tag{54}$$

where $A_2(\nu)$ comes from the form of Chapman and Cowling,[S58] not the value $A^{(2)}(n)$ of Hirschfelder.[S59] Variable cancellation yields

$$\eta^* = F_{\eta,\mathrm{IPL}}(n)(T^*)^{\frac{1}{2}+\frac{2}{n}} \tag{55}$$

with

$$F_{\eta,\mathrm{IPL}}(n) = \frac{5\left(\frac{2}{n}\right)^{2/n}}{8\sqrt{\pi}A_2(\nu = n+1)\Gamma\left(4-\frac{2}{n}\right)}. \tag{56}$$

Similar for self-diffusion, from Hirschfelder,[S60] with $\mu = \frac{1}{2}m$ for pure component self-diffusion:

$$D = \frac{\frac{3}{16}\sqrt{\frac{4k_\mathrm{B}^3}{\pi m}}\left(\frac{k_\mathrm{B}}{n\varepsilon\sigma^n}\right)^{2/n} T^{\frac{3}{2}+\frac{2}{n}}}{pA_1(\nu = n+1)\Gamma(3-\frac{2}{n})/2^{2/n}} \tag{57}$$

where again, $A_1(\nu)$ comes from the form of Chapman and Cowling,[S58] not the value $A^{(1)}(n)$ of Hirschfelder.[S61] With $p = \rho_\mathrm{N} k_\mathrm{B} T$, and variable cancellation, the result is

$$\rho^* D^* = F_{D,\mathrm{IPL}}(n)(T^*)^{\frac{1}{2}+\frac{2}{n}} \tag{58}$$

with

$$F_{D,\mathrm{IPL}}(n) = \frac{3}{8\sqrt{\pi}}\frac{(2/n)^{2/n}}{A_1(\nu = n+1)\Gamma(3-\frac{2}{n})} \tag{59}$$

4.3 Collision Integral

Starting off with Enskog dilute-gas viscosity in engineering and simulation units

$$\eta_{\rho_\mathrm{N}\to 0,\mathrm{IPL}} = \frac{5}{16\sigma^2}\left(\frac{mk_\mathrm{B}T}{\pi}\right)^{1/2}\frac{1}{\Omega^{(2,2)*}} \tag{60}$$

$$\eta^*_{\rho_\mathrm{N}\to 0,\mathrm{IPL}} = \frac{5}{16}\left(\frac{T^*}{\pi}\right)^{1/2}\frac{1}{\Omega^{(2,2)*}}, \tag{61}$$

after substitution of LHS completely

$$\frac{5\left(\frac{2}{n}\right)^{2/n}(T^*)^{2/n+1/2}}{8\sqrt{\pi}A_2(\nu = n+1)\Gamma\left(4-\frac{2}{n}\right)} = \frac{5}{16}\left(\frac{T^*}{\pi}\right)^{1/2}\frac{1}{\Omega^{(2,2)*}}, \tag{62}$$

the collision integral $\Omega^{(2,2)*}$ is equal to

$$\Omega^{(2,2)*} = \frac{1}{2}\frac{A_2(\nu = n+1)\Gamma\left(4-\frac{2}{n}\right)}{\left(\frac{2}{n}\right)^{2/n}(T^*)^{2/n}} \tag{63}$$

The reader should be cautioned that the term $A_2(n)$, in some cases (e.g., Hirschfelder,[S56] Amdur and Mason[S63]) differs by a factor of $2^{2/n}$ due to its definition, here we use the definition of Chapman and Cowling.[S58]

The same derivation for the self-diffusion yields:

$$(\rho_{\mathrm{N}} D)_{\rho\to 0} = \frac{3}{8\sigma^2}\left(\frac{k_{\mathrm{B}}T}{m\pi}\right)^{1/2}\frac{1}{\Omega^{(1,1)*}} \tag{64}$$

$$(\rho^* D^*)_{\rho\to 0} = \frac{3}{8}\left(\frac{T^*}{\pi}\right)^{1/2}\frac{1}{\Omega^{(1,1)*}} \tag{65}$$

and after substitution of the LHS completely

$$\frac{3}{8\sqrt{\pi}}\frac{(2/n)^{2/n}(T^*)^{\frac{1}{2}+\frac{2}{n}}}{A_1(\nu=n+1)\Gamma(3-\frac{2}{n})} = \frac{3}{8}\left(\frac{T^*}{\pi}\right)^{1/2}\frac{1}{\Omega^{(1,1)*}}, \tag{66}$$

the collision integral $\Omega^{(1,1)*}$ is given by

$$\Omega^{(1,1)*} = \frac{A_1(\nu=n+1)\Gamma\left(3-\dfrac{2}{n}\right)}{\left(\dfrac{2}{n}\right)^{2/n}(T^*)^{2/n}} \tag{67}$$

The reader should be cautioned that the term $A_1(n)$, in some cases (e.g., Hirschfelder,[S56] Amdur and Mason[S64]) differs by a factor of $2^{2/n}$ due to its definition, here we use the definition of Chapman and Cowling.[S58]

4.4 Scaled zero-density transport properties

The value of η^+ in the zero-density limit is given by (see Eq. (53))

$$\lim_{\rho\to 0}\eta^+_{\mathrm{IPL}} = \frac{F_{\eta,\mathrm{IPL}}(n)(T^*)^{2/n+1/2}}{\sqrt{T^*}}(\bar{B}_2(1-3/n))^{2/3}(T^*)^{-2/n} \tag{68}$$

which after cancellation yields

$$\lim_{\rho\to 0}\eta^+_{\mathrm{IPL}} = F_{\eta,\mathrm{IPL}}(n)(\bar{B}_2(1-3/n))^{2/3}, \tag{69}$$

where $F_{\eta,\mathrm{IPL}}$ comes from Eq. (56). In perfect analogy, the zero-density limit value for D^+ is given by

$$\lim_{\rho\to 0}D^+_{\mathrm{IPL}} = F_{D,\mathrm{IPL}}(n)(\bar{B}_2(1-3/n))^{2/3}. \tag{70}$$

where $F_{D,\mathrm{IPL}}$ comes from Eq. (59).

The values of the scaled zero-density-limit transport properties for the IPL potential are plotted in Fig. S9, and tabular values are given in Table S5.

Table S5: Calculated values of A_1, A_2, $\lim_{\rho\to 0} D^+$ and $\lim_{\rho\to 0} \eta^+$ for the IPL potential. The values of A_1 and A_2 follow the definitions of Chapman and Cowling.[S58] Values of A_1 and A_2 (with the same definition) are also presented in Rosenfeld,[S67] but the column headings are erroneously inverted in that work.

n	A_1	A_2	$\lim_{\rho\to 0} D^+$	$\lim_{\rho\to 0} \eta^+$
4	0.4219402	0.4361951	0.408922	0.263706
6	0.3854373	0.3567499	0.382047	0.257981
8	0.3807996	0.330403	0.371785	0.259693
10	0.3834267	0.3187256	0.366335	0.262322
12	0.3880369	0.3128182	0.362929	0.264822
14	0.3930631	0.3096396	0.360583	0.26701
20	0.4068599	0.3065779	0.356481	0.271888
24	0.4143952	0.3065549	0.354904	0.274144

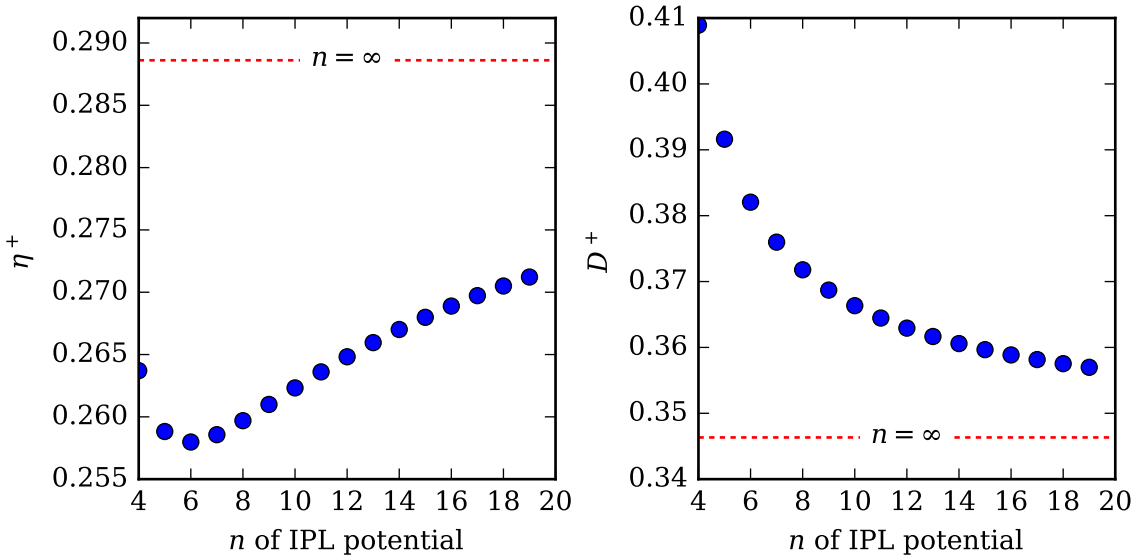

Figure S9: Zero-density limit of inverse-power-law potentials

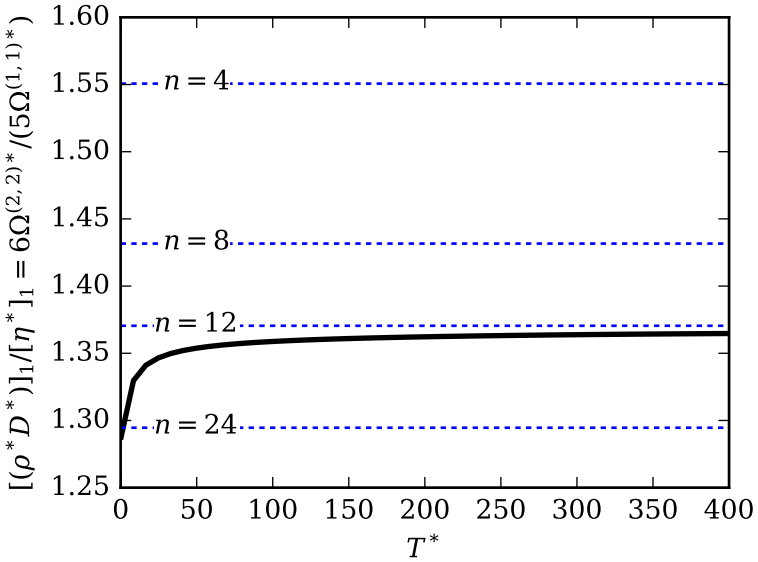

Figure S10: Ratio of $[(\rho^* D^*)]_1/[\eta^*]_1$ for Lennard-Jones and IPL potentials. Solid black line is the Lennard-Jones 12-6 potential, dashed blue lines are the IPL potentials.

4.4.1 Python/sympy code for calculating A_l

```
"""
Python 3+ only!
"""
import scipy.integrate
import numpy as np
import mpmath
def _A_l(*,nu,l):
    """
    Actually do the calculation for A_l, with the independent variable
    nu, where nu = n+1
    All arguments are passed as keyword arguments
    """
    def integrand(v0):
        o = lambda v: 1-v**2-2/(nu-1)*(v/v0)**(nu-1)
        def get_v00(v0):
            if isinstance(nu,int) and nu < 30:
                c = np.zeros((nu,))
                c[-1] = 1 # Constant term
                c[-3] = -1 #
                c[0] = -2/(nu-1)/v0**(nu-1)
                roots = np.roots(c)
                root = roots[np.isreal(roots) & (roots>0)]
                assert(len(root)==1)
                return np.real(root[0])
            else:
                # General treatment with mpmath
                lower, upper = (1e-16, 10)
                return mpmath.findroot(o, (lower, upper), solver='bisect',
    verbose=False)
        def chi(v0):
            def inner(v):
                return (1-v**2-2/(nu-1)*(v/v0)**(nu-1))**-0.5
            v00 = get_v00(v0)
            val, err = scipy.integrate.quad(inner, 0, v00)
            return np.pi-2*val
        return (1-np.cos(chi(v0))**l)*v0
    val, err = scipy.integrate.quad(integrand, 0, np.inf)
    return val
A_l_vals = {}
def A_l(*,nu=None,n=None,l=2):
    """
    Main function to calculate the term A_l as defined by Chapman and
   Cowling
    All arguments are to be passed as keyword arguments.
    If the value has already been calculated, it is cached for speed
    l must be provided, and one of nu OR n
    """
    # Convert inputs to nu, if n is provided
    if (nu is not None and n is None):
        # Nothing to do, not strictly necessary, but useful
        # for cleaning up the logical flow
        pass
    elif nu is None and n is not None:
        nu = n+1
    else:
        raise ValueError()
    if (nu,l) not in A_l_vals:
        A_l_vals[(nu,l)] = _A_l(nu=nu,l=l)
    return A_l_vals[(nu,l)]
```

5 The High-Temperature Limit

Correlations for the collision integrals for the Lennard-Jones 12-6 fluid are available in Kim and Monroe.[S1] Additionally, an analytic (though requiring numerical integration) solution for $\Omega^{(2,2)*}$ for the family of IPL potentials is available above. Figure S11a presents the $\Omega^{(2,2)*}$ collision integral for the Lennard-Jones 12-6 fluid along with the values obtained for the IPL potentials, and Figure S11b does the same for the $\Omega^{(1,1)*}$ collision integral. Up to the stated maximum of the correlation of $T^* = 400$, the collision integrals are slowly approaching the collision integral of the $n = 12$ IPL, as expected. In the region of extrapolation above $T^* \geq 400$, the collision integral sharply decreases in value, eventually crossing into the negative region. A negative collision integral value is simply a consequence of Kim and Monroe not constraining the behavior of the collision integral formulation to smoothly transition to the $n = 12$ IPL potential in the infinite temperature limit. Temperatures on the order of $T^* = 10^5$ are admittedly well beyond the region where the Lennard-Jones 12-6 potential is a reasonable model for real molecules; at these temperatures molecules would have been fully ionized.

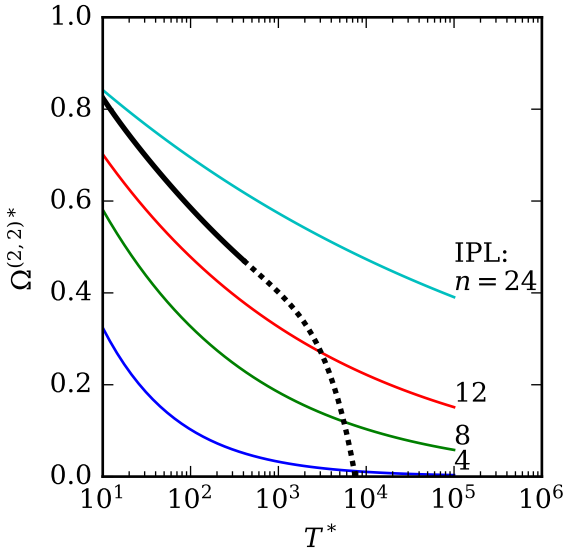

(a) Collision integral $\Omega^{(2,2)*}$.

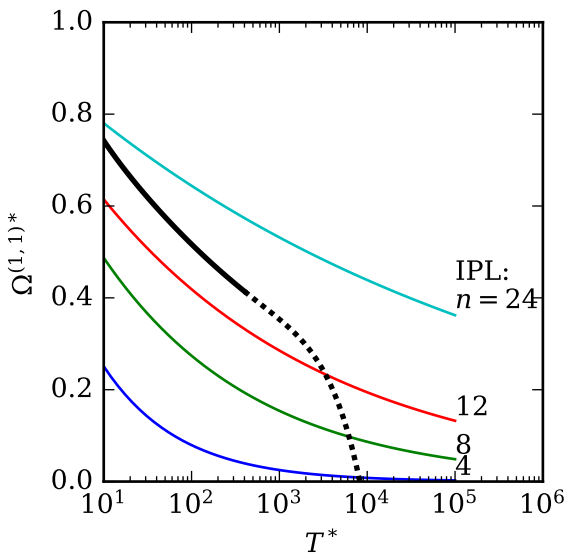

(b) Collision integral $\Omega^{(1,1)*}$.

Figure S11: Collision integrals $\Omega^{(l,s)*}$ for the full Lennard-Jones 12-6 potential from the correlation of Kim and Monroe[S1] (in black) as well as the solutions for four hardnesses of the IPL potential (in colors). The solid part of the curve corresponds to the range of validity $0.3 \leq T^* \leq 400$, and the range above $T^* = 400$ corresponds to extrapolation of the correlation beyond its range of applicability.

5.1 Rosenfeld re-derivation

The scaled viscosity of the IPL fluid is given by

$$\eta^*_{\mathrm{IPL}} = F_{\eta,\mathrm{IPL}}(n)(T^*)^{\frac{2}{n}+\frac{1}{2}} \tag{71}$$

In macroscopically-reduced units, we have

$$\tilde{\eta}_{\mathrm{IPL}} = \frac{\eta^*_{\mathrm{IPL}}}{(\rho^*)^{2/3}(T^*)^{1/2}} = \frac{F_{\eta,\mathrm{IPL}}(n)}{\gamma^{2/3}} \tag{72}$$

because $\gamma = \rho^*(T^*)^{-3/n}$, therefore $(\rho^*)^{2/3} = \gamma^{2/3}(T^*)^{2/n}$. All the temperature dependence cancels. If then the evaluation of Eq. (9) is carried out for the IPL potential, truncated at the first virial coefficient, with the virial coefficients evaluated from Eq. (52),

$$\frac{-s^{\mathrm{r}}}{k_{\mathrm{B}}} = \rho^* \left[T^* \left(\frac{\mathrm{d}B^*_2}{\mathrm{d}T^*} \right) + B^*_2 \right] \tag{73}$$

$$= \rho^* \left(\bar{B}_2(1-3/n)(T^*)^{-3/n} \right) \tag{74}$$

$$= \bar{B}_2\gamma(1-3/n) \tag{75}$$

Therefore, in the virial expansion truncated after the first term,

$$\gamma^{-2/3} = \left(\frac{\bar{B}_2(1-3/n)}{(-s^{\mathrm{r}}/k_{\mathrm{B}})} \right)^{2/3} \tag{76}$$

and substitution yields

$$\tilde{\eta}_{\mathrm{IPL}} = F_{\eta,\mathrm{IPL}}(n)\bar{B}_2(1-3/n)(-s^{\mathrm{r}}/k_{\mathrm{B}})^{-2/3} = \left(\lim_{\rho\to 0} \eta^+_{\mathrm{IPL}} \right) (-s^{\mathrm{r}}/k_{\mathrm{B}})^{-2/3} \tag{77}$$

from which the result of Rosenfeld is obtained:

$$\tilde{\eta}_{\mathrm{IPL}} \propto (-s^{\mathrm{r}}/k_{\mathrm{B}})^{-2/3}. \tag{78}$$

For self-diffusion, the same derivation is needed, and $F_{\eta,\mathrm{IPL}}$ is replaced with $F_{\mathrm{D,IPL}}$.

6 EoS from Thol et al.

Both of the multiparameter equations of state developed by Thol[S68,S69] are formulated in terms of the Helmholtz energy with density ρ^* and reciprocal temperature $(T^*)^{-1}$ as independent variables. Since the Helmholtz energy is a fundamental property, all thermodynamic state properties can by calculated by a combination of partial derivatives with respect to the independent variables. In general, the derivatives are defined as follows

$$\widetilde{A}_{ij} = \tau^i \delta^j \left(\frac{\partial^{i+j} \alpha^{\mathrm{r}}}{\partial \tau^i \partial \delta^j} \right), \tag{79}$$

where $\tau = T_{\mathrm{c}}^*/T^*$, and $\delta = \rho^*/\rho_{\mathrm{c}}^*$. Derivatives of the ideal part are marked with the superscript "0", whereas the residual part is labeled with "r".

Some useful thermodynamic properties needed for the calculation of the thermal conductivity are the

$$\text{isochoric heat capacity: } c_v^* = -(\widetilde{A}_{20}^0 + \widetilde{A}_{20}^{\mathrm{r}}) \tag{80}$$

$$\text{isobaric heat capacity: } c_p^* = c_v^* + \frac{(1 + \widetilde{A}_{01}^{\mathrm{r}} - \widetilde{A}_{11}^{\mathrm{r}})^2}{1 + 2\widetilde{A}_{01}^{\mathrm{r}} + \widetilde{A}_{02}} \tag{81}$$

$$\text{compressibility: } \left(\frac{\partial p^*}{\partial \rho^*} \right)_{T^*} = T^*[1 + 2\widetilde{A}_{01}^{\mathrm{r}} + \widetilde{A}_{02}^{\mathrm{r}}] \tag{82}$$

The quantities marked with an asterisk are reduced quantities defined by $T^* = T/(\varepsilon/k_{\mathrm{B}})$, $p^* = p\sigma^3/\varepsilon$, $c_p^* = c_p/k_{\mathrm{B}}$, $c_v^* = c_v/k_{\mathrm{B}}$, where c_p and c_v are per particle quantities.

6.1 Virial coefficients

The second thermal virial coefficient B_2^* is equal to

$$B_2^* = \lim_{\rho_{\mathrm{N}} \to 0} \left(\frac{\partial \alpha^{\mathrm{r}}}{\partial \rho^*} \right)_{T^*} = \lim_{\rho_{\mathrm{N}} \to 0} \left(\frac{\partial \alpha^{\mathrm{r}}}{\partial \delta} \right)_{\tau} \left(\frac{\partial \delta}{\partial \rho^*} \right) \tag{83}$$

with the equation of state given by a form similar to

$$\begin{aligned} \alpha^{\mathrm{r}} = & \sum_{k=1}^{n_p} N_k \delta^{d_k} \tau^{t_k} \\ & + \sum_{k=1+n_p}^{1+n_p+n_e} N_k \delta^{d_k} \tau^{t_k} \exp(-\delta^{l_k}) \\ & + \sum_{k=2+n_p+n_e}^{1+n_p+n_e+n_g} N_k \delta^{d_k} \tau^{t_k} \exp(-\eta_k(\delta - \varepsilon_k)^2 - \beta_k(\tau - \gamma_k)^2) \end{aligned} \tag{84}$$

and its first δ partial derivative given by

$$\left(\frac{\partial \alpha^{\mathrm{r}}}{\partial \delta}\right)_{\tau} = \sum_{k=1}^{n_p} N_k \delta^{d_k-1} \tau^{t_k} d_k + \sum_{k=1+n_p}^{1+n_p+n_e} N_k \delta^{d_k-1} \tau^{t_k} \exp(-\delta^{l_k})[d_k - l_k \delta^{l_k}] + \sum_{k=2+n_p+n_e}^{1+n_p+n_e+n_g} N_k \delta^{d_k-1} \tau^{t_k} \exp(-\eta_k(\delta-\varepsilon_k)^2 - \beta_k(\tau-\gamma_k)^2)[d_k - 2\eta_k\delta(\delta-\varepsilon_k)] \tag{85}$$

For this property, only the terms that result in a meaningful contribution to δ have to be considered. Therefore we keep terms with $d_k = 1$, because they yield 0^0=1 in the limit of zero density ($\delta = 0$) for the derivative $\partial\alpha^{\mathrm{r}}/\partial\delta$. Higher order exponents always lead to $0^q = 0$ for $q > 1$.

Figure S12 presents the comparison between the virial contributions at high temperatures for both the $n = 12$ IPL potential and the Lennard-Jones 12-6 potential. Though at first glance the infinite temperature limit seems correct, the two models cross at a temperature on the order of $T^* = 10^6$, beyond which they head in different directions.

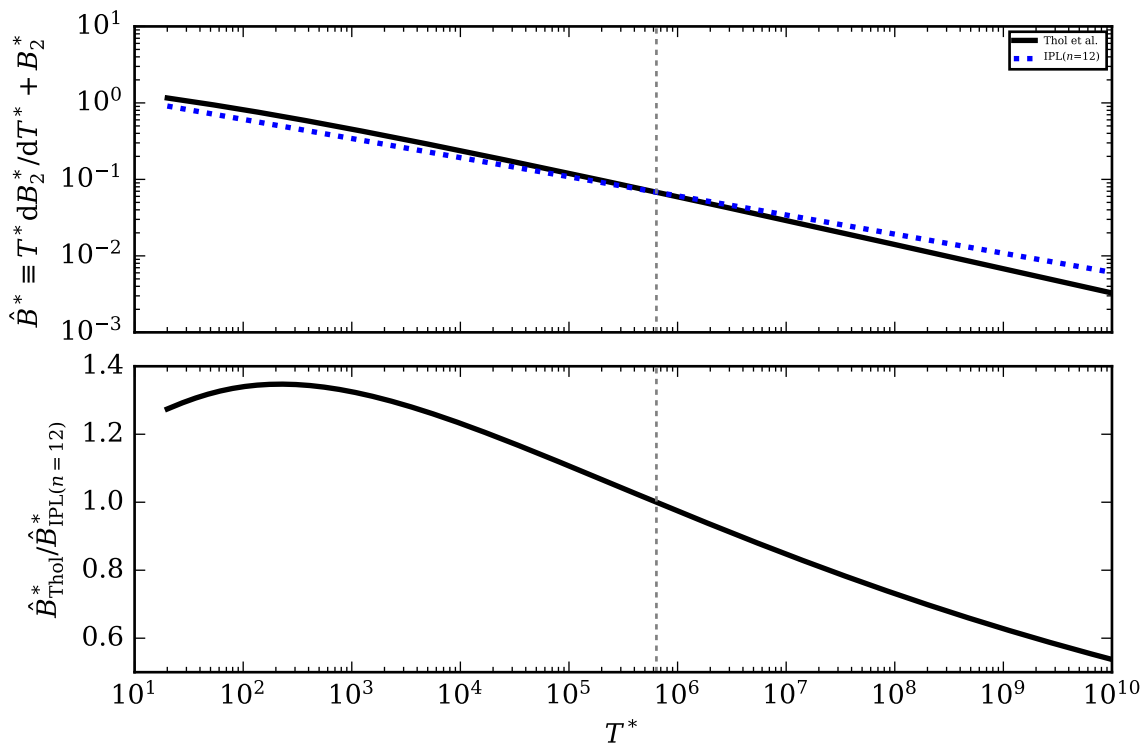

Figure S12: Comparison of the equation of state of Thol et al.[S69] and the $n = 12$ limit for the virial coefficient contribution to the +-scaled transport properties

Nonetheless, the equation of state of Thol et al.[S69] provides the best qualitative behav-

ior of the virial coefficients in the high temperature limit of any empirical model for the Lennard-Jones potential in the literature that does not yield the correct virial coefficients by construction (Fig. S13). Here we consider the MBWR model of Pieprzyk,[S70] but their P1P2 model should in theory reproduce the exact virial coefficients of[S71] to arbitrary precision. No validation data or verification code to that effect was provided in.[S70]

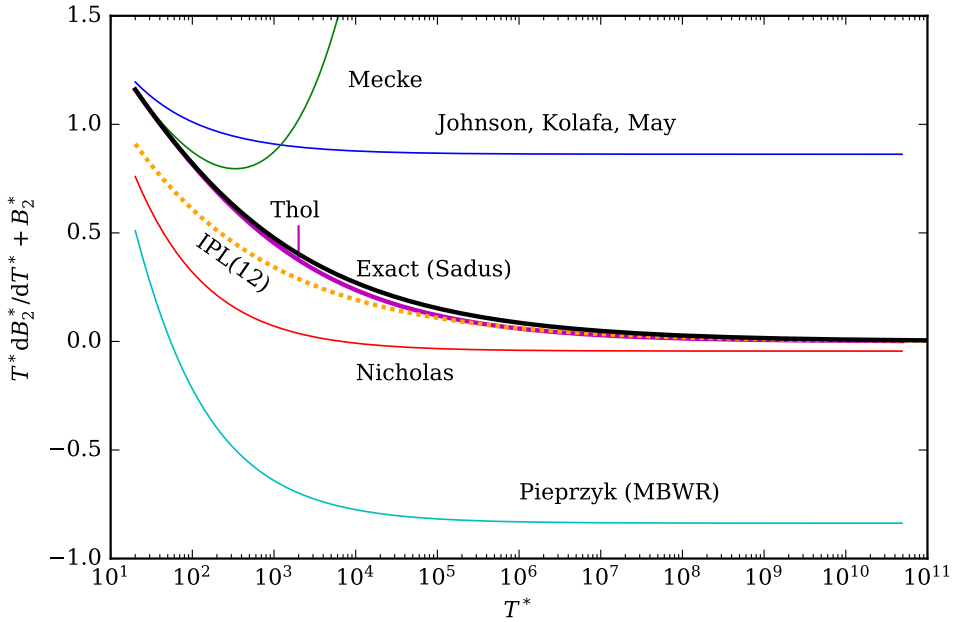

Figure S13: Comparison of the empirical equations of state in the infinite temperature limit for the virial coefficient contribution to the +-scaled transport properties

7 Comparisons with existing correlations from the literature

In this section, we present deviation plots from the Lennard-Jones transport property correlations that are available in the literature. Some general notes on the plots in this section:

- Any values outside the range of ±1000% have been plotted at ±1000%, but their true value is used to calculate the error metrics.
- The dashed cyan vertical lines show the approximate location of the liquidus and solidus lines
- For thermal conductivity, the dashed black vertical lines show the residual entropy values at the critical points corresponding to the LJTS and LJT equations of state.
- In some cases where large deviations are present, a symmetric-logarithmic y-axis is used, with a linear scale from -20% to 20% and a logarithmic scale outside that range.

7.1 Viscosity

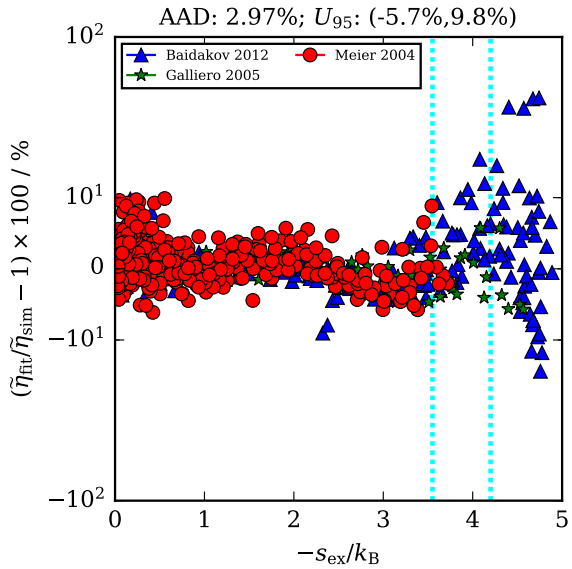

(a) The primary datasets

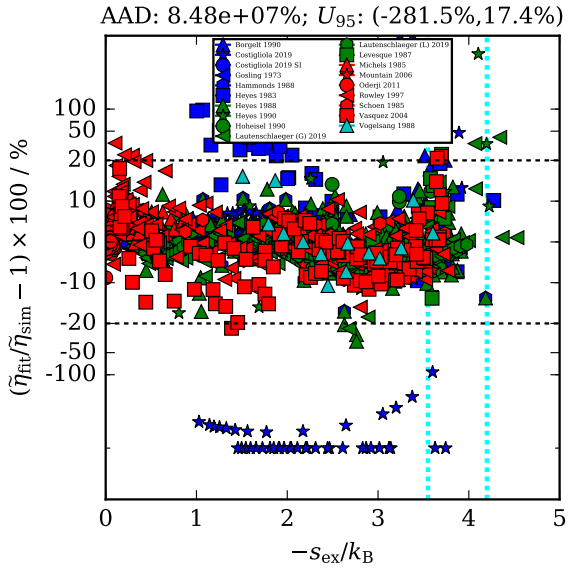

(b) The secondary datasets

Figure S14: Results from the correlation of Galliero et al.[S27]

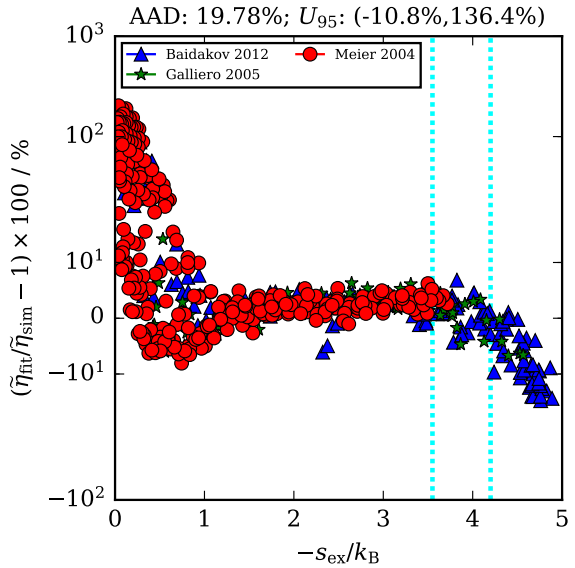

(a) The primary datasets

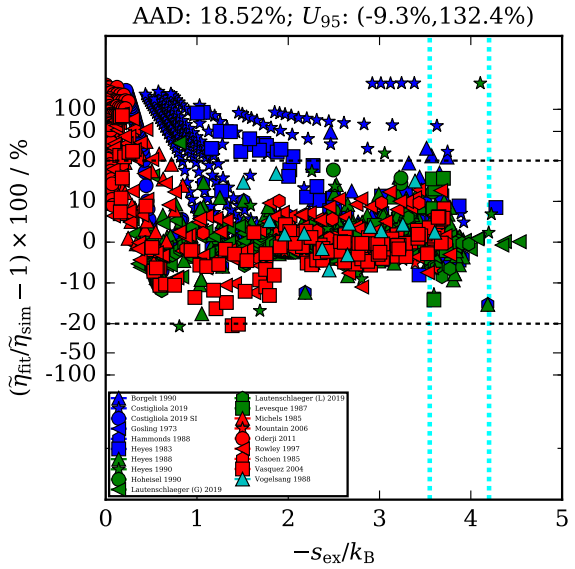

(b) The secondary datasets

Figure S15: Results from the correlation of Lautenschlaeger and Hasse.[S10]

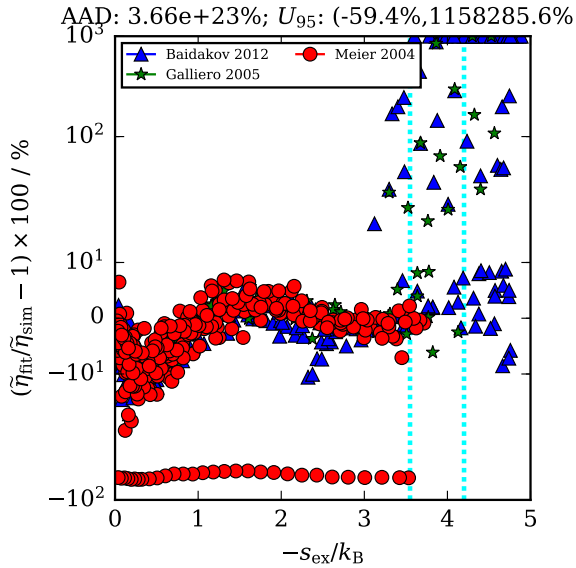

(a) The primary datasets

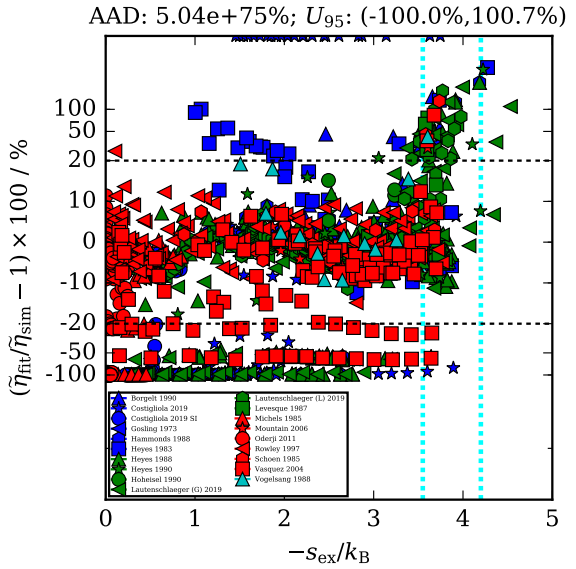

(b) The secondary datasets

Figure S16: Results from the correlation of Rowley and Painter.[S14]

7.2 Conductivity

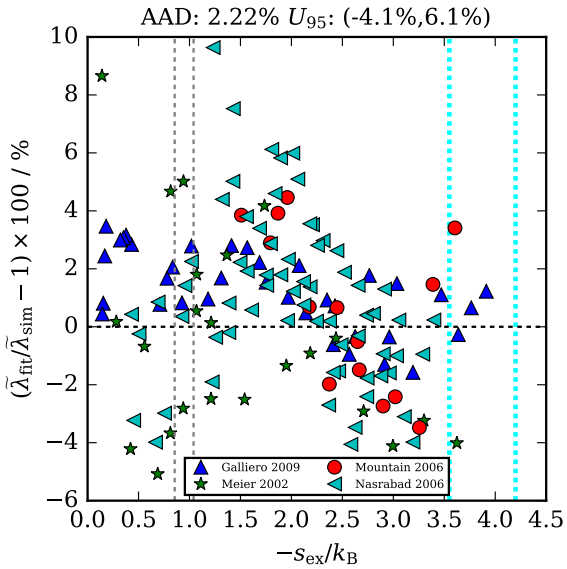

(a) The primary datasets

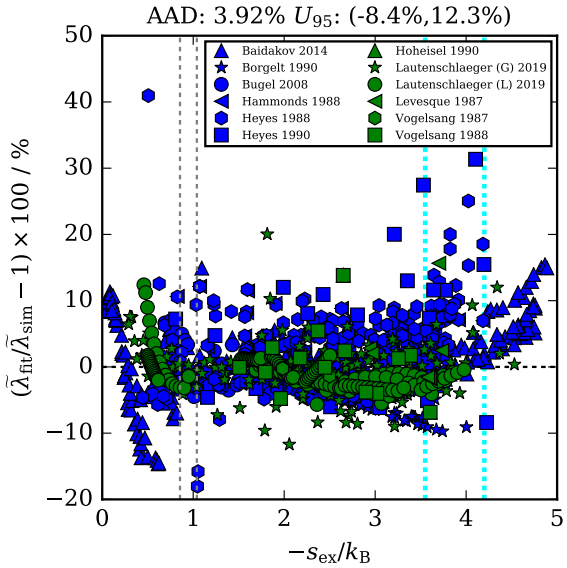

(b) The secondary datasets

Figure S17: Results from the correlation of Galliero and Boned.[S18]

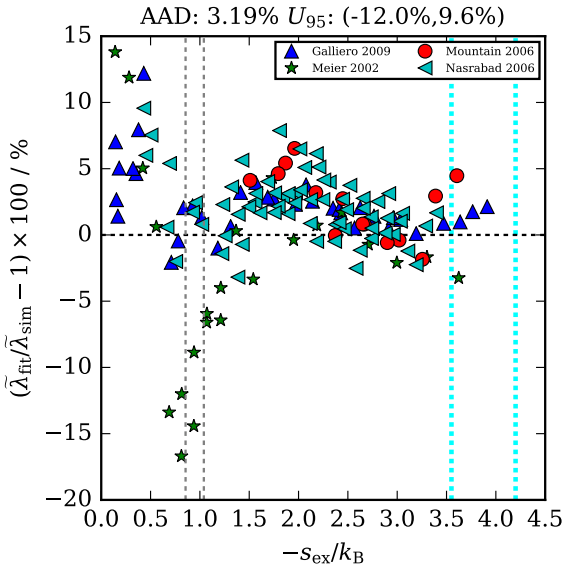

(a) The primary datasets

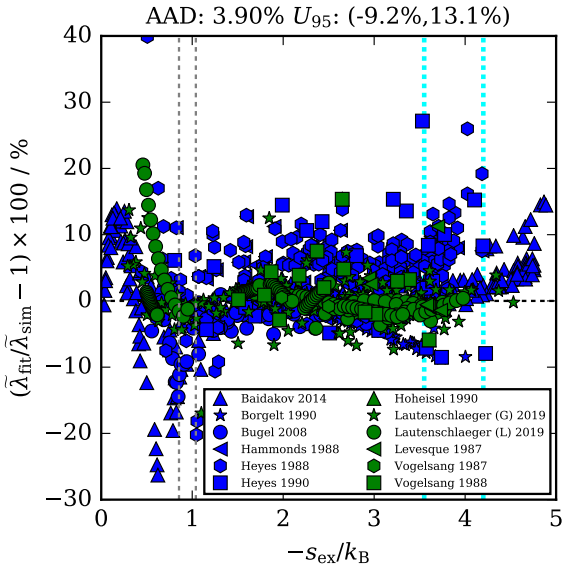

(b) The secondary datasets

Figure S18: Results from the correlation of Lautenschlaeger and Hasse.[S10]

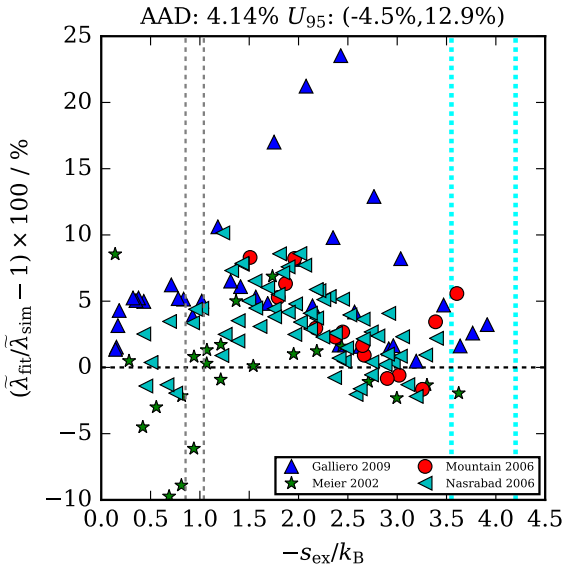

(a) The primary datasets

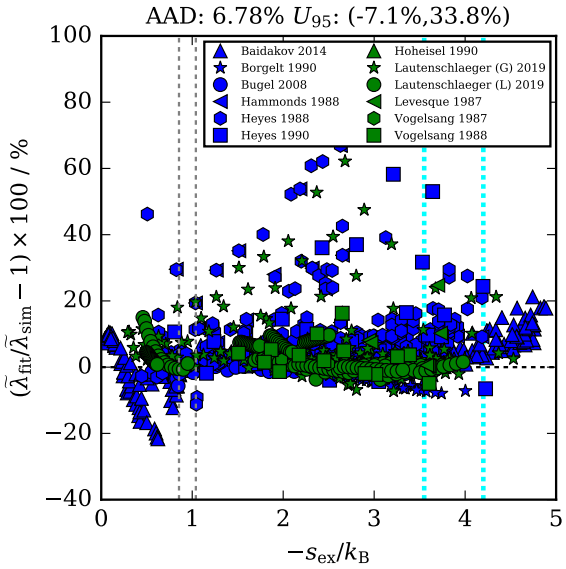

(b) The secondary datasets

Figure S19: Results from the correlation of Bugel and Galliero.[S17]

7.3 Self-Diffusion

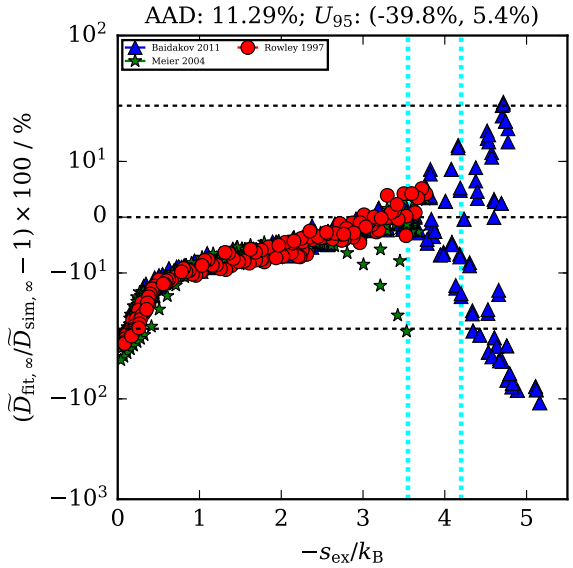

(a) The primary datasets

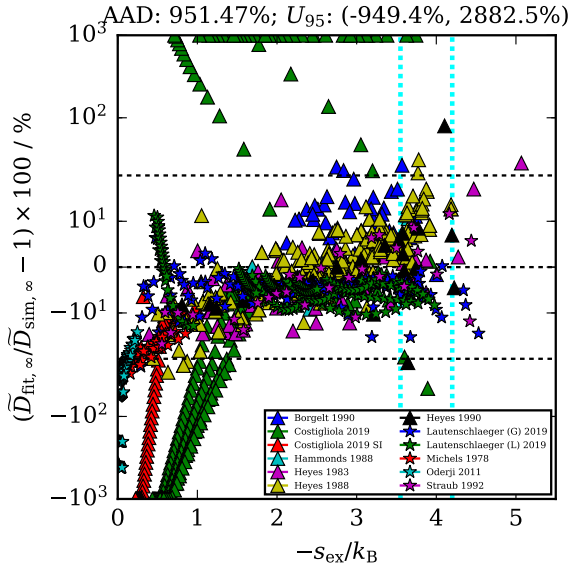

(b) The secondary datasets

Figure S20: Results from the correlation of Lautenschlaeger and Hasse.[S10]

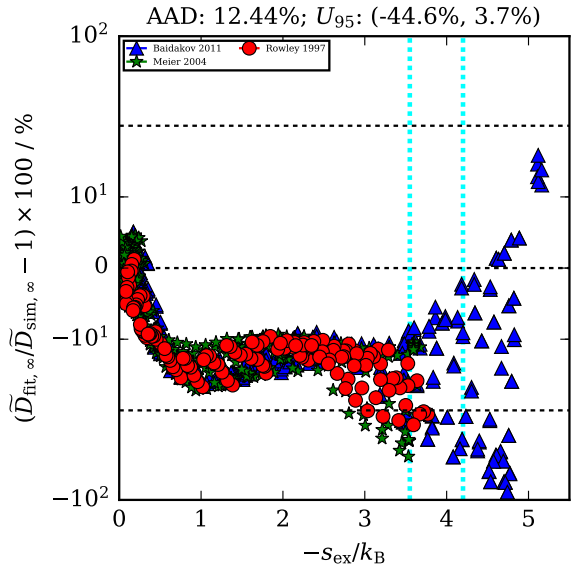

(a) The primary datasets

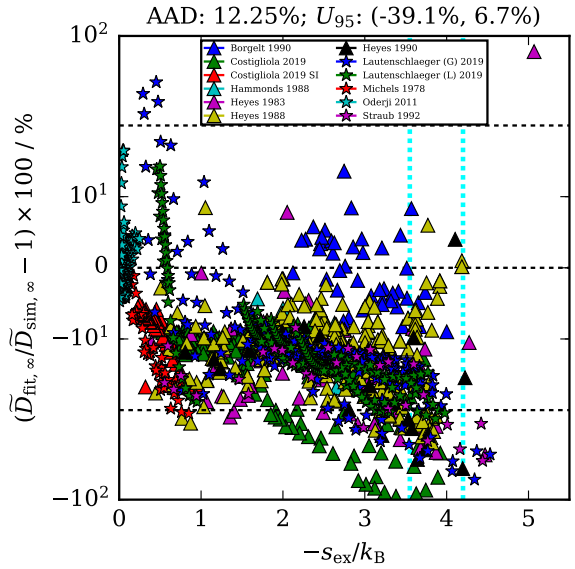

(b) The secondary datasets

Figure S21: Results from the correlation of Ruckenstein and Liu.[S72]

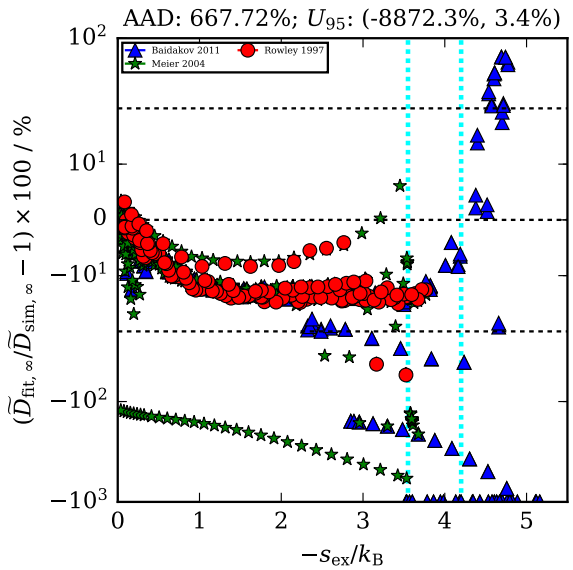

(a) The primary datasets

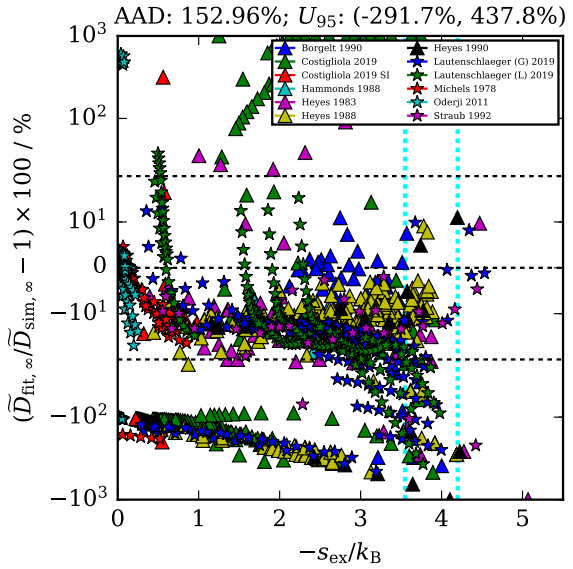

(b) The secondary datasets

Figure S22: Results from the correlation of Rowley and Painter.[S14]

8 Verification Data

Also included in the SI is a Python script called `implementation.py`. That file includes all the correlations, and auto-generated the data in Table S6. The script uses only functionality found in the standard library of Python and the `numpy` library for linear algebra.

Please note that the implementation uses the equation of state for the full Lennard-Jones 12-6 potential of Thol et al.[S69]

Table S6: Verification data to ensure correct implementation. Large number of significant digits provided is to ensure correct implementation and is not indicative of the uncertainty in the calculated parameters

T^*	ρ^*	$-s_{\mathrm{ex}}/k_{\mathrm{B}}$	η^*	λ^*	$\rho^* D^*$
1.4	0.0	-0.0	0.5799287054157818	2.17507407450368	0.7646575954423214
1.4	0.4	1.050964300807837	0.4112265798032804	1.9119361936263055	0.19006346942550134
0.8	0.0	-0.0	0.8926626216861204	3.347623987348237	1.1896537025627558
0.8	0.7	2.531251343524489	1.2068761923853173	4.450359284997936	0.06877274587113219

References

(S1) Kim, S. U.; Monroe, C. W. High-accuracy Calculations of Sixteen Collision Integrals for Lennard-Jones (12–6) Gases and Their Interpolation to Parameterize Neon, Argon, and Krypton. *J. Comput. Phys.* **2014**, *273*, 358–373, DOI: 10.1016/j.jcp.2014.05.018.

(S2) Olchowy, G. A.; Sengers, J. V. A Simplified Representation for the Thermal Conductivity of Fluids in the Critical Region. *Int. J. Thermophys.* **1989**, *10*, 417–426, DOI: 10.1007/bf01133538.

(S3) Baidakov, V.; Protsenko, S.; Kozlova, Z. The Self-Diffusion Coefficient in Stable and Metastable States of the Lennard–Jones Fluid. *Fluid Phase Equilib.* **2011**, *305*, 106–113, DOI: 10.1016/j.fluid.2011.03.002.

(S4) Borgelt, P.; Hoheisel, C.; Stell, G. Exact Molecular Dynamics and Kinetic Theory Results for Thermal Transport Coefficients of the Lennard-Jones Argon Fluid in a Wide Region of States. *Phys. Rev. A* **1990**, *42*, 789–794, DOI: 10.1103/physreva.42.789.

(S5) Costigliola, L.; Pedersen, U. R.; Heyes, D. M.; Schrøder, T. B.; Dyre, J. C. Communication: Simple Liquids' High-Density Viscosity. *J. Chem. Phys.* **2018**, *148*, 081101, DOI: 10.1063/1.5022058.

(S6) Hammonds, K. D.; Heyes, D. M. Transport Coefficients of Model Simple Liquids. A Molecular-Dynamics Study and Effective Hard-Sphere Analysis. *Journal of the Chemical Society, Faraday Transactions 2* **1988**, *84*, 705–725, DOI: 10.1039/f29888400705.

(S7) Heyes, D. M. Self-Diffusion and Shear Viscosity of Simple Fluids. A Molecular-Dynamics Study. *Journal of the Chemical Society, Faraday Transactions 2* **1983**, *79*, 1741–1758, DOI: 10.1039/f29837901741.

(S8) Heyes, D. M. Transport Coefficients of Lennard-Jones Fluids: A Molecular-Dynamics and Effective-Hard-Sphere Treatment. *Phys. Rev. B* **1988**, *37*, 5677–5696, DOI: 10.1103/physrevb.37.5677.

(S9) Heyes, D.; Powles, J. Information Theory Applied to the Transport Coefficients of Lennard-Jones Fluids. *Mol. Phys.* **1990**, *71*, 781–800, DOI: 10.1080/00268979000102111.

(S10) Lautenschlaeger, M. P.; Hasse, H. Transport Properties of the Lennard-Jones Truncated and Shifted Fluid from Non-Equilibrium Molecular Dynamics Simulations. *Fluid Phase Equilib.* **2019**, *482*, 38–47, DOI: 10.1016/j.fluid.2018.10.019.

(S11) Meier, K.; Laesecke, A.; Kabelac, S. Transport Coefficients of the Lennard-Jones Model Fluid. II Self-Diffusion. *J. Chem. Phys.* **2004**, *121*, 9526–9535, DOI: 10.1063/1.1786579.

(S12) Michels, J.; Trappeniers, N. The Self-Diffusion Coefficient in the Gas Phase at Moderate Densities, Obtained by Computer Simulations. *Physica A* **1978**, *90*, 179–195, DOI: 10.1016/0378-4371(78)90108-5.

(S13) Oderji, H. Y.; Ding, H.; Behnejad, H. Calculation of the Second Self-Diffusion and Viscosity Virial Coefficients of Lennard-Jones Fluid by Equilibrium Molecular Dynamics Simulations. *Phys. Rev. E* **2011**, *83*, 061202, DOI: 10.1103/physreve.83.061202.

(S14) Rowley, R. L.; Painter, M. M. Diffusion and Viscosity Equations of State for a Lennard-Jones Fluid Obtained from Molecular Dynamics Simulations. *Int. J. Thermophys.* **1997**, *18*, 1109–1121, DOI: 10.1007/bf02575252.

(S15) Straub, J. E. Analysis of the Role of Attractive Forces in Self-Diffusion of a Simple Fluid. *Mol. Phys.* **1992**, *76*, 373–385, DOI: 10.1080/00268979200101391.

(S16) Baidakov, V. G.; Protsenko, S. P. Metastable Lennard-Jones Fluids. II. Thermal Conductivity. *J. Chem. Phys.* **2014**, *140*, 214506, DOI: 10.1063/1.4880958.

(S17) Bugel, M.; Galliero, G. Thermal Conductivity of the Lennard-Jones Fluid: An Empirical Correlation. *Chem. Phys.* **2008**, *352*, 249–257, DOI: 10.1016/j.chemphys.2008.06.013.

(S18) Galliero, G.; Boned, C. Thermal Conductivity of the Lennard-Jones Chain Fluid Model. *Phys. Rev. E* **2009**, *80*, 061202, DOI: 10.1103/physreve.80.061202.

(S19) Hoheisel, C. Memory Functions and the Calculation of Dynamical Properties of Atomic Liquids. *Comp. Phys. Rep.* **1990**, *12*, 29–66, DOI: 10.1016/0167-7977(90)90003-o.

(S20) Levesque, D.; Verlet, L. Molecular Dynamics Calculations of Transport Coefficients. *Mol. Phys.* **1987**, *61*, 143–159, DOI: 10.1080/00268978700101041.

(S21) Meier, K. Computer Simulation and Interpretation of the Transport Coefficients of the Lennard-Jones Model Fluid. Ph.D. thesis, University of the Federal Armed Forces Hamburg, 2002.

(S22) Mountain, R. D. System Size and Control Parameter Effects in Reverse Perturbation Nonequilibrium Molecular Dynamics. *J. Chem. Phys.* **2006**, *124*, 104109, DOI: 10.1063/1.2178340.

(S23) Nasrabad, A. E.; Laghaei, R.; Eu, B. C. Molecular Theory of Thermal Conductivity of the Lennard-Jones Fluid. *J. Chem. Phys.* **2006**, *124*, 084506, DOI: 10.1063/1.2166394.

(S24) Vogelsang, R.; Hoheisel, C.; Ciccotti, G. Thermal Conductivity of the Lennard-Jones Liquid by Molecular Dynamics Calculations. *J. Chem. Phys.* **1987**, *86*, 6371–6375, DOI: 10.1063/1.452424.

(S25) Vogelsang, R.; Hoheisel, G.; Luckas, M. Shear Viscosity and Thermal Conductivity of the Lennard-Jones Liquid Computed Using Molecular Dynamics and Predicted by a Memory Function Model for a Large Number of States. *Mol. Phys.* **1988**, *64*, 1203–1213, DOI: 10.1080/00268978800100813.

(S26) Baidakov, V. G.; Protsenko, S. P.; Kozlova, Z. R. Metastable Lennard-Jones Fluids. I. Shear Viscosity. *J. Chem. Phys.* **2012**, *137*, 164507, DOI: 10.1063/1.4758806.

(S27) Galliéro, G.; Boned, C.; Baylaucq, A. Molecular Dynamics Study of the Lennard-Jones Fluid Viscosity: Application to Real Fluids. *Ind. Eng. Chem. Res.* **2005**, *44*, 6963–6972, DOI: 10.1021/ie050154t.

(S28) Gosling, E. M.; McDonald, I.; Singer, K. On the Calculation by Molecular Dynamics of the Shear Viscosity of a Simple Fluid. *Mol. Phys.* **1973**, *26*, 1475–1484, DOI: 10.1080/00268977300102631.

(S29) Meier, K.; Laesecke, A.; Kabelac, S. Transport Coefficients of the Lennard-Jones Model Fluid. I. Viscosity. *J. Chem. Phys.* **2004**, *121*, 3671, DOI: 10.1063/1.1770695.

(S30) Michels, J.; Trappeniers, N. Molecular Dynamical Calculations of the Viscosity of Lennard-Jones Systems. *Physica A* **1985**, *133*, 281–290, DOI: 10.1016/0378-4371(85)90067-6.

(S31) Schoen, M.; Hoheisel, C. The Shear Viscosity of a Lennard-Jones Fluid Calculated by Equilibrium Molecular Dynamics. *Mol. Phys.* **1985**, *56*, 653–672, DOI: 10.1080/00268978500102591.

(S32) Vasquez, V. R.; Macedo, E. A.; Zabaloy, M. S. Lennard-Jones Viscosities in Wide Ranges of Temperature and Density: Fast Calculations Using a Steady–State Periodic Perturbation Method. *Int. J. Thermophys.* **2004**, *25*, 1799–1818, DOI: 10.1007/s10765-004-7736-3.

(S33) Lautenschlaeger, M. P.; Horsch, M.; Hasse, H. Simultaneous Determination of Thermal Conductivity and Shear Viscosity Using Two-Gradient Non-Equilibrium Molecular Dynamics Simulations. *Mol. Phys.* **2019**, *117*, 189–199, DOI: 10.1080/00268976.2018.1504134.

(S34) Hafskjold, B.; Ikeshoji, T.; Ratkje, S. K. On the Molecular Mechanism of Thermal Diffusion in Liquids. *Mol. Phys.* **1993**, *80*, 1389–1412, DOI: 10.1080/00268979300103101.

(S35) Berendsen, H. J. C.; Postma, J. P. M.; van Gunsteren, W. F.; DiNola, A.; Haak, J. R. Molecular Dynamics with Coupling to an External Bath. *J. Chem. Phys.* **1984**, *81*, 3684–3690, DOI: 10.1063/1.448118.

(S36) Evans, R.; Hansen, J.-P.; Löwen, H. Foreword. *J. Phys.: Condens. Matter* **2002**, *14*, DOI: 10.1088/0953-8984/14/46/001.

(S37) Evans, D. J. Homogeneous NEMD Algorithm for Thermal Conductivity-Application of Non-Canonical Linear Response Theory. *Phys. Lett. A* **1982**, *91*, 457–460, DOI: 10.1016/0375-9601(82)90748-4.

(S38) Evans, D. J. Thermal Conductivity of the Lennard-Jones Fluid. *Phys. Rev. A* **1986**, *34*, 1449–1453, DOI: 10.1103/PhysRevA.34.1449.

(S39) Evans, D. J.; Morriss, G. P. *Statistical Mechanics of Nonequilibrium Liquids*; Academic Press, 1990; p 302, DOI: 10.1016/B978-0-12-244090-8.50003-5.

(S40) Nosé, S. A Unified Formulation of the Constant Temperature Molecular Dynamics Methods. *J. Chem. Phys.* **1984**, *81*, 511–519, DOI: 10.1063/1.447334.

(S41) Hoover, W. G. Canonical Dynamics: Equilibrium Phase-Space Distributions. *Phys. Rev. A* **1985**, *31*, 1695–1697, DOI: 10.1103/PhysRevA.31.1695.

(S42) Bedrov, D.; Smith, G. D. Thermal Conductivity of Molecular Fluids from Molecular Dynamics Simulations: Application of a New Imposed-Flux Method. *J. Chem. Phys.* **2000**, *113*, 8080–8084, DOI: 10.1063/1.1312309.

(S43) Müller-Plathe, F. A Simple Nonequilibrium Molecular Dynamics Method for Calculating the Thermal Conductivity. *J. Chem. Phys.* **1997**, *106*, 6082–6085, DOI: 10.1063/1.473271.

(S44) Müller-Plathe, F. Reversing the Perturbation in Nonequilibrium Molecular Dynamics: An Easy Way to Calculate the Shear Viscosity of Fluids. *Phys. Rev. E* **1999**, *59*, 4894–4898, DOI: 10.1103/PhysRevE.59.4894.

(S45) Bordat, P.; Müller-Plathe, F. The Shear Viscosity of Molecular Fluids: A Calculation by Reverse Nonequilibrium Molecular Dynamics. *J. Chem. Phys.* **2002**, *116*, 3362–3369, DOI: 10.1063/1.1436124.

(S46) Evans, M.; Heyes, D. Combined Shear and Elongational Flow by Non-Equilibrium Molecular Dynamics. *Mol. Phys.* **1990**, *69*, 241–263, DOI: 10.1080/00268979000100171.

(S47) Daivis, P. J.; Todd, B. D. A Simple, Direct Derivation and Proof of the Validity of the SLLOD Equations of Motion for Generalized Homogeneous Flows. *J. Chem. Phys.* **2006**, *124*, 194103, DOI: 10.1063/1.2192775.

(S48) Hess, B. Determining the Shear Viscosity of Model Liquids from Molecular Dynamics Simulations. *J. Chem. Phys.* **2002**, *116*, 209–217, DOI: 10.1063/1.1421362.

(S49) Bussi, G.; Donadio, D.; Parrinello, M. Canonical Sampling through Velocity Rescaling. *J. Chem. Phys.* **2007**, *126*, 014101, DOI: 10.1063/1.2408420.

(S50) Costigliola, L.; Heyes, D. M.; Schrøder, T. B.; Dyre, J. C. Revisiting the Stokes-Einstein Relation without a Hydrodynamic Diameter. *J. Chem. Phys.* **2019**, *150*, 021101, DOI: 10.1063/1.5080662.

(S51) Costigliola, L. RUC Glass and Time Data Repository, Accessed on January 14, 2019. 2019; http://glass.ruc.dk/data/.

(S52) Yeh, I.-C.; Hummer, G. System-Size Dependence of Diffusion Coefficients and Viscosities from Molecular Dynamics Simulations with Periodic Boundary Conditions. *J. Phys. Chem. B* **2004**, *108*, 15873–15879, DOI: 10.1021/jp0477147.

(S53) Barlow, N. S.; Schultz, A. J.; Weinstein, S. J.; Kofke, D. A. An Asymptotically Consistent Approximant Method with Application to Soft- and Hard-Sphere Fluids. *J. Chem. Phys.* **2012**, *137*, 204102, DOI: 10.1063/1.4767065.

(S54) Sherwood, A. E.; Mason, E. A. Virial Coefficients for the Exponential Repulsive Potential. *Phys. Fluids* **1965**, *8*, 1577–1579, DOI: 10.1063/1.1761466.

(S55) Ref. S54, Eq. 16.

(S56) Hirschfelder, J. O.; Curtiss, C. F.; Bird, R. B. *Molecular Theory of Gases and Liquids*; John Wiley and Sons, 1954.

(S57) Ref. S56, Eq. 8.3-6.

(S58) Chapman, S.; Cowling, T. G. *The Mathematical Theory of Non-uniform Gases: An Account of the Kinetic Theory of Viscosity, Thermal Conduction and Diffusion in Gases*; Cambridge University Press, 1970.

(S59) Ref. S56, Table 8.3-3.

(S60) Ref. S56, Eq. 8.3-6.

(S61) Ref. S56, Table 8.3-3.

(S62) Amdur, I.; Mason, E. A. Properties of Gases at Very High Temperatures. *Phys. Fluids* **1958**, *1*, 370, DOI: 10.1063/1.1724353.

(S63) Ref. S62, Eq. 24.

(S64) Ref. S62, Eq. 24.

(S65) Rosenfeld, Y. A Quasi-universal Scaling Law for Atomic Transport in Simple Fluids. *J. Phys.: Condens. Matter* **1999**, *11*, 5415–5427, DOI: 10.1088/0953-8984/11/28/303.

(S66) Ref. S65, Table 3.

(S67) Ref. S65, Table 3.

(S68) Thol, M.; Rutkai, G.; Span, R.; Vrabec, J.; Lustig, R. Equation of State for the Lennard-Jones Truncated and Shifted Model Fluid. *Int. J. Thermophys.* **2015**, *36*, 25–43, DOI: 10.1007/s10765-014-1764-4.

(S69) Thol, M.; Rutkai, G.; Köster, A.; Lustig, R.; Span, R.; Vrabec, J. Equation of State for the Lennard-Jones Fluid. *J. Phys. Chem. Ref. Data* **2016**, *45*, 023101, DOI: 10.1063/1.4945000.

(S70) Pieprzyk, S.; Brańka, A. C.; Maćkowiak, S.; Heyes, D. M. Comprehensive Representation of the Lennard-Jones Equation of State Based on Molecular Dynamics Simulation Data. *J. Chem. Phys.* **2018**, *148*, 114505, DOI: 10.1063/1.5021560.

(S71) Heyes, D. M.; Rickayzen, G.; Pieprzyk, S.; Brańka, A. C. The Second Virial Coefficient and Critical Point Behavior of the Mie Potential. *J. Chem. Phys.* **2016**, *145*, 084505, DOI: 10.1063/1.4961653.

(S72) Ruckenstein, E.; Liu, H. Self-Diffusion in Gases and Liquids. *Ind. Eng. Chem. Res.* **1997**, *36*, 3927–3936, DOI: 10.1021/ie9701332.